A detailed description of the solar wind triggers of two dayside transients: Events of 25 July 1997

Eftyhia Zesta
Department of Atmospheric Sciences, University of California, Los Angeles, Los Angeles, California, USA

David G. Sibeck
NASA Goddard Space Flight Center, Greenbelt, Maryland, USA

Received 28 January 2003; revised 11 September 2003; accepted 15 September 2003; published 6 January 2004.

[1] Traveling Convection Vortices (TCVs), a specific type of dayside transient event, offer a good opportunity to study the modes of interaction between the solar wind, bow shock and the magnetosphere/ionosphere system. We study here in detail the solar wind triggers of two TCV events that occurred at 1500 UT and 1835 UT on 25 July 1997. During these two events there was a fortuitous conjunction of four solar wind monitors near the Earth's magnetosphere. We were able to identify the exact solar wind discontinuity that triggered each ground TCV. We found that the 1500 UT TCV was triggered by the density (and thus dynamic pressure) enhancement accompanying a tangential discontinuity. We were able to determine the orientation of the discontinuity plane and thus predict, in good agreement with observations, the propagation of the discontinuity between the four spacecraft as well as the propagation of the transient in the magnetosphere (geosynchronous) and ionosphere. The ground transient was generated in the early afternoon local time and then propagated westward, first toward local noon and then away from noon toward dawn. The 1835 UT TCV, which was stronger, was triggered by a more complicated solar wind discontinuity that exhibited significant spatial structure and an unusual propagation pattern. A detailed analysis of the orientation of the discontinuity fronts explained the propagation of the discontinuity in the solar wind. Even though the discontinuity did not carry a significant dynamic pressure enhancement, it had the properties required to generate a hot flow anomaly (HFA) or a foreshock cavity at the bow shock. The corresponding pressure reduction in the magnetosheath interacted with the magnetosphere to generate the transient near local noon that propagates eastward toward dusk. Geosynchronous observations confirm these conclusions. To strengthen our conclusions, we compared the discontinuity that triggered the ground TCV event with four other discontinuities that occurred in the same 2-hour window. We found that none of the other four discontinuities carried significant dynamic pressure enhancements or had properties required to create a HFA at the bow shock. They did not trigger detectable transients on the ground. It thus seems that TCVs can be triggered by solar wind discontinuities that either carry dynamic pressure enhancements (or alternatively reductions) or by discontinuities that create HFAs or foreshock cavities at the bow shock. *INDEX TERMS:* 2784 Magnetospheric Physics: Solar wind/magnetosphere interactions; 2724 Magnetospheric Physics: Magnetopause, cusp, and boundary layers; 2109 Interplanetary Physics: Discontinuities; 2736 Magnetospheric Physics: Magnetosphere/ionosphere interactions; *KEYWORDS:* dayside transients, traveling convection vortices, hot flow anomaly, foreshock cavities, solar wind triggering

Citation: Zesta, E., and D. G. Sibeck (2004), A detailed description of the solar wind triggers of two dayside transients: Events of 25 July 1997, *J. Geophys. Res.*, *109*, A01201, doi:10.1029/2003JA009864.

1. Introduction

[2] The solar wind couples with the magnetosphere in a dynamic and transient way owing to the numerous small-scale (of the order of only several minutes) structures advected with the solar wind, propagating through the solar wind, or alternatively created by the interaction of the interplanetary magnetic field with the bow shock. As a result there are a variety of transient perturbations observed at the high-latitude dayside ionosphere (as recorded in ground magnetograms), where the coupling of the solar wind with the magnetosphere is most direct and field lines map in the outer magnetosphere and magnetopause.

0148-0227/04/2003JA009864

[3] The subject of the solar wind sources and triggers of dayside transients observed on the ground is still very controversial and there is no consensus in the field, mostly due to lack of appropriate solar wind data. The few prior studies, both statistical and case studies, have used only a single solar wind monitor and often in far from ideal location for observing the correlated triggers of dayside transients. Statistical studies of high-latitude transient events [e.g., *Z.-M. Lin et al.*, 1995; *Konik et al.*, 1994; *Sibeck and Korotova.*, 1996; *Sitar et al.*, 1996] have shown contradictory results. *Konik et al.* [1994] and *Z.-M. Lin et al.* [1995] find that the majority of their events are due to pulsed reconnection, while *Sibeck and Korotova* [1996] find that most of their events correlate with sharp IMF orientation changes. *Sibeck and Korotova* [1996] suggest an interpretation of their events in terms of a model in which changes in the IMF orientation at the bow shock generate pressure variations in the magnetosheath. While the above-mentioned studies identified transient events on the ground and then looked for correlated solar wind and IMF signatures, *Sitar et al.* [1996] did the reverse study; they identified sharp solar wind pressure changes and investigated their effect on the ground. Sitar et al. clearly identified a ground response to solar wind pressure increases and decreases but were unable to find any consistent relationship between the pressure change and the characteristics of the ground response. *Sitar et al.* [1996] also reported no agreement between the actual ground response and the one predicted from theoretical models [*Glassmeier et al.*, 1989; *Kivelson and Southwood*, 1991; *Lysak et al.*, 1994].

[4] Some case studies were successful in establishing correlation with solar wind triggers [e.g., *Friis-Christensen et al.*, 1988; *Zesta et al.*, 1999] but by using single point measurements these studies were not able to fully characterize the solar wind discontinuities that trigger the ground transients. *Sibeck et al.* [1999] used two solar wind monitors to present a comprehensive study of the magnetospheric response to a tangential discontinuity that created a hot flow anomaly (HFA) while interacting with the bow shock, which in turn triggered a strong TCV on the ground. The ground response was also studied by *Sitar et al.* [1998]. HFAs are a type of diamagnetic cavity observed very near the bow shock and result from the interaction of certain interplanetary current sheets with the bow shock. Usually, the current sheet is a tangential discontinuity, but that is not a necessary condition. The observed characteristics of HFAs include central regions with hot, tenuous plasma with largely disturbed magnetic fields and deflected flow velocities and durations of a few minutes [see *Schwartz et al.*, 2000, and references therein]. The study of *Sibeck et al.* [1999] has opened the way for a possible reconciliation of the results of prior statistical studies on the sources of TCVs and MIEs. It indicated that structures like HFA created and localized in the bow shock region may be the primary trigger of TCVs. In a more recent work, *Sibeck et al.* [2002] find that foreshock cavities (similar to but without the high temperatures of HFAs) are much more common than HFAs and suggest that they also trigger transients on the ground.

[5] In summary, while prior work on the solar wind triggers of TCVs was unclear and contradictory, more recent work seems to indicate that the bow shock plays an essential role in forming the disturbances that impact the magnetopause and trigger the ground transients. The question remains if all ground transients are triggered by foreshock processes or some of them are also triggered by advected solar wind disturbances and how important each contribution is. Even more, we must consider that the solar wind and IMF are often highly dynamic and continuously changing, and disturbances appear random. It is therefore nontrivial to find a convincing correlation between a particular solar wind disturbance and a ground transient. Still one must do more than that; one must ultimately predict which solar wind disturbances will create transients in the magnetosphere and which will not, if the interaction is properly understood.

[6] In the present study we offer, for the first time, a detailed analysis of the solar wind discontinuities that trigger two ground transients on 25 July 1997, using four different solar wind and magnetosheath monitors. We were able to show that the first TCV was triggered by a pristine solar wind disturbance, a tangential discontinuity advected with the solar wind, while the second TCV was triggered by either a HFA or a foreshock cavity, a disturbance created at the bow shock. We were able to test our conclusions by analyzing a 2-hour period of solar wind data and predicting correctly which disturbances would trigger ground transients.

2. The 1500 UT Discontinuity: Trigger of the First Ground Transient

2.1. Transient on the Ground

[7] We used magnetometers from the Greenland, MACCS, and CANOPUS chains to identify the transient on the ground and verify that it is a traveling convection vortex. Figure 1 shows a map of the ground magnetometers in these chains (solid circles) and the ionospheric footprint of the GOES 8 and 9 spacecraft (solid diamonds). The dashed lines are lines of geographic latitude and longitude, while the solid lines are lines of constant geomagnetic latitude from 60° to 85° geomagnetic latitude. The geomagnetic longitude lines at 90° and −70° longitude are also plotted in the figure.

[8] The ground transient is observed in all three magnetometer chains. MACCS and CANOPUS cover the whole morning sector, from dawn to noon, and Greenland is in the early afternoon sector, 1200–1500 MLT. Figure 2 shows data from a representative set of magnetometers lying near 73°–74° magnetic latitude (where TCVs are known to reach their peak amplitude) and covering 10 hours in MLT. The stations are stacked from top to bottom from the easternmost (SCO, a Greenland station) to the westernmost (CONT, a CANOPUS station). The MLT of each station at 1500 UT is noted over each station trace in Figure 2. The onset of the TCV is at ∼1450 UT at SCO, in the early afternoon sector, and it then propagates westward. It reaches peak amplitude of ∼150 nT at ∼0930 MLT at the station of CH and then weakens as it continues propagating westward. We measure the peak amplitude from the B_y (east-west) component in Figure 2 because this component measures the strength of the north-south current between the vortices and has the same phase at all stations observing the TCV. The amplitude of the B_x (north-south) component strongly depends on how far north or south the station is from the

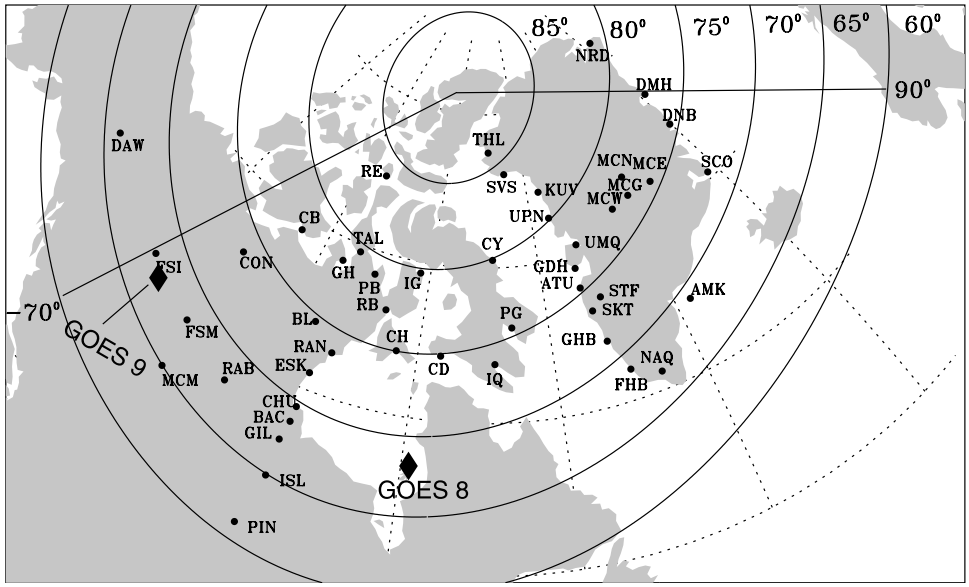

Figure 1. Map of the ground magnetometers (solid circles) of the MACCS, CANOPUS, and Greenland chains, and the ionospheric footprint of the Goes 8 and 9 spacecraft (black diamonds).

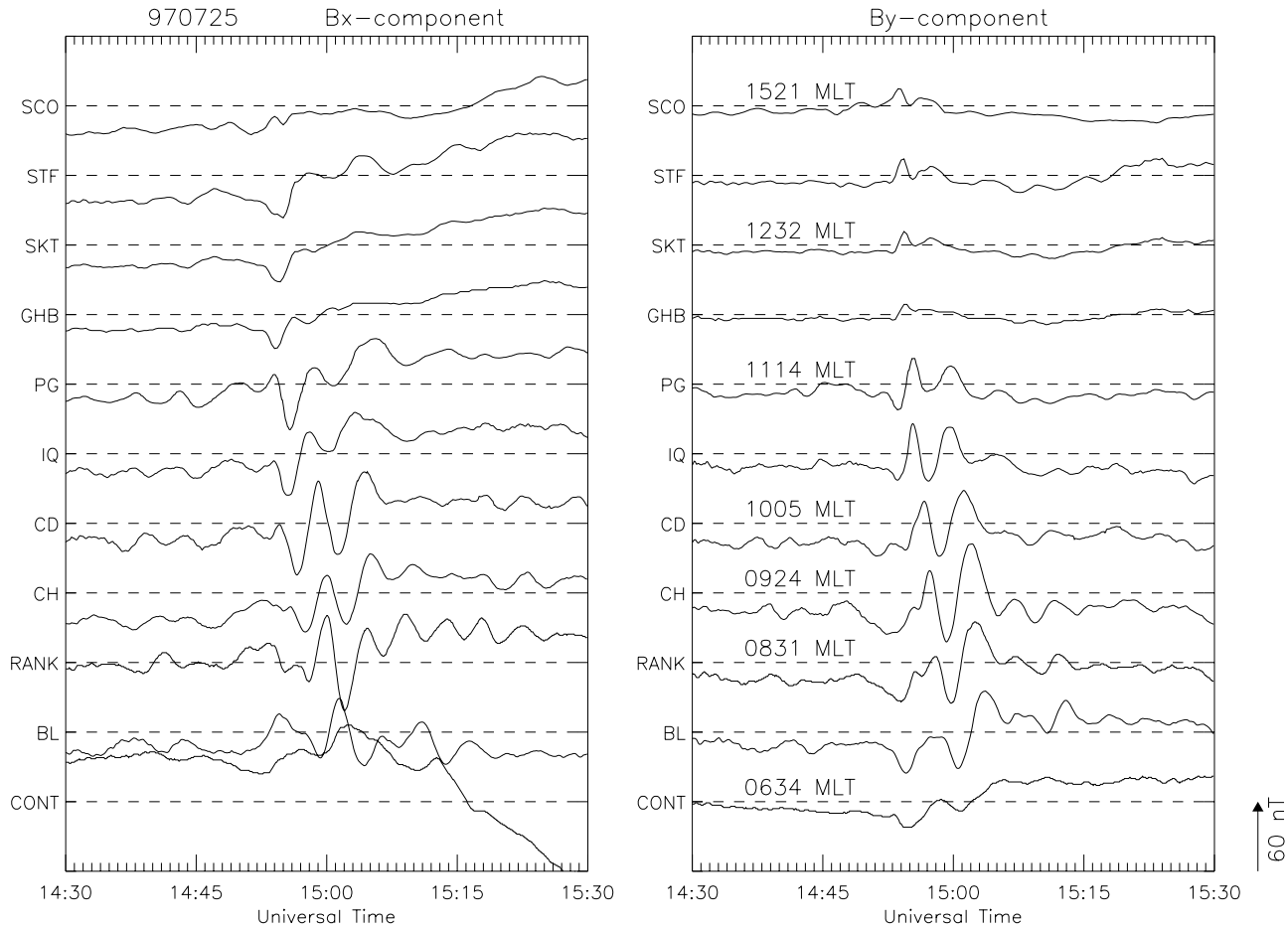

Figure 2. The 1500 UT TCV from a set of ground magnetometers lying near 74° magnetic latitude and covering ~10 hours in MLT. Stations are aligned from top to bottom from the easternmost stations to the westernmost station.

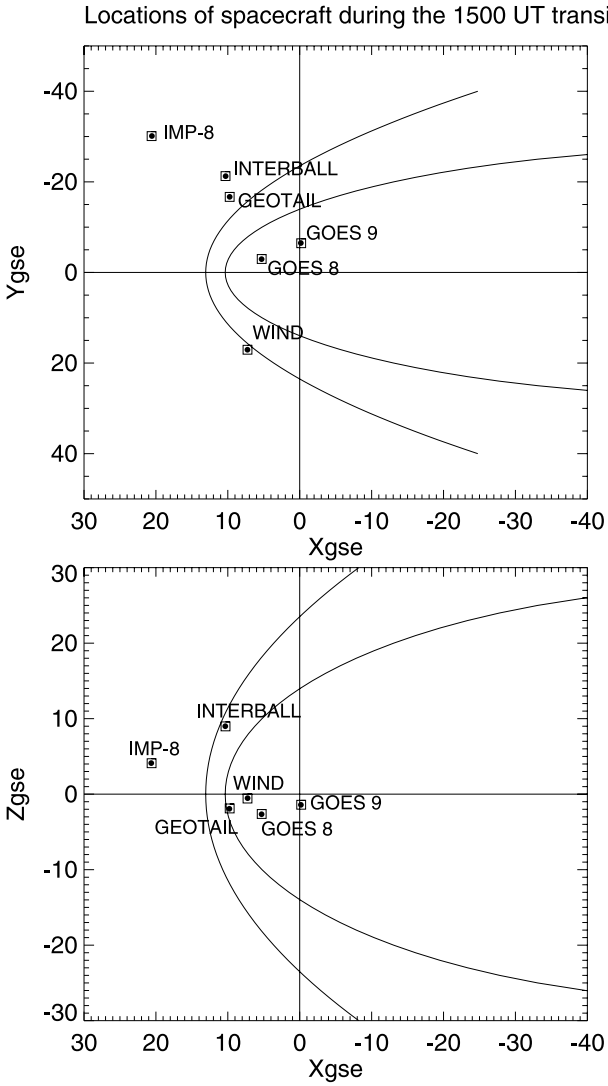

Figure 3. The location of the four solar wind monitors and the two GOES spacecraft in the XY and XZ GSE planes.

vortex centers, and it is thus less reliable for measuring the evolution of the strength of the propagating TCV. The equivalent current pattern in the ionosphere (not shown) is that of a westward-propagating twin vortex with a downward field-aligned current at the center of the leading clockwise vortex and an upward field aligned current at the center of the trailing counterclockwise vortex. Therefore, this event is a typical traveling convection vortex (TCV).

2.2. Solar Wind and IMF Data

[9] At the time of the first TCV event there were four solar wind monitors: Wind, Geotail, Interball, and IMP 8 upstream from the bow shock. Figure 3 shows the locations of the four solar wind spacecraft in the XY and XZ GSE planes. We determined the location of the magnetopause and bow shock using code that (1) for the magnetopause location is based on the results of *Roelof and Sibeck* [1993], and (2) for the bow shock simply scales the *Fairfield* [1971] model bow shock to the observed solar wind dynamic pressure. All four spacecraft are within 10 R_E of the ecliptic plane (Wind and Geotail are within only 3 R_E). Wind is in the late afternoon upstream region, Interball and Geotail are in the upstream morning foreshock region, and IMP 8 is in the same local time as Geotail and Interball but further upstream of the bow shock. The locations of the two geosynchronous GOES 8 and 9 spacecraft are also shown in Figure 3.

[10] Figure 4 shows the solar wind plasma and IMF observations at (a) Wind, (b) Geotail, (c) Interball, and (d) IMP 8 at times surrounding the 1500 UT ground TCV event. In Figure 4a we plot from top to bottom: the proton density, the dynamic pressure, the x, y, and z components of the solar wind velocity, the magnetic field magnitude |B|, and its x, y, and z components. All vector quantities are plotted in the Geocentric Solar Ecliptic (GSE) coordinate system. The plasma data are from the 3DP plasma instrument [*R. P. Lin et al.*, 1995] and the IMF observations are from the magnetic field experiment [*Lepping et al.*, 1995] on Wind. The time resolution for both the plasma and the magnetic field data is ~3 s. The onset of the discontinuity we believe responsible for the ground TCV is at 1447:30 UT and is marked by the vertical dashed line in Figure 4a. The discontinuity consists of an increase in density and dynamic pressure, a decrease in the magnetic field strength, and a rotation of the magnetic field direction primarily in the XY plane (inspecting a much longer time period than the one shown in Figure 4a, we determined that this rotation is a heliospheric current sheet crossing).

[11] Figure 4b shows the plasma and IMF data observed at Geotail during a similar time period. The same quantities as in Figure 4a are plotted. The solar wind plasma moments are from the Comprehensive Plasma Instrument (CPI) solar wind analyzer [*Frank et al.*, 1994] and have a ~49 s time resolution. The magnetic field measurements [*Kokubun et al.*, 1994] have a ~3 s time resolution. A similar discontinuity to that at Wind was observed at Geotail with an onset at 1454:30 UT, marked by the vertical dashed line. The onset of the discontinuity is determined from the magnetic field data as the plasma data have a much lower resolution, ~49 s. Just as in the Wind observations, we see an increase in density and dynamic pressure, a decrease in magnetic field, and a rotation of the magnetic field in the XY plane. However, there are some differences between the signature at Geotail and that at Wind. The rotation of the magnetic field at Geotail occurs in two clear steps and the density enhancement seems to coincide with the second step of the magnetic field rotation, not with the onset of the discontinuity (although the latter is not as clear with only 49 s resolution plasma data). These differences must be due to spatial structure in the discontinuity front. In addition, Geotail is in the foreshock, as evidenced by the strong waves seen in the magnetic field up to ~1510 UT. Therefore the discontinuity signature has been altered by its proximity to the bow shock and the interaction with the foreshock strong wave activity.

[12] Figure 4c shows data from Interball. High time resolution ion plasma data are only available from the VDP instrument that measures the total flux ($n \cdot \mathbf{V}$). The instrument has five sensors (only four of them are operating and are shown), and each detector measures the total ion flux and the electron flux of electrons with energies ≥170 eV [*Šafránková et al.*, 1997]. VDP0 always looks sunward (thus measuring the bulk of the oncoming solar

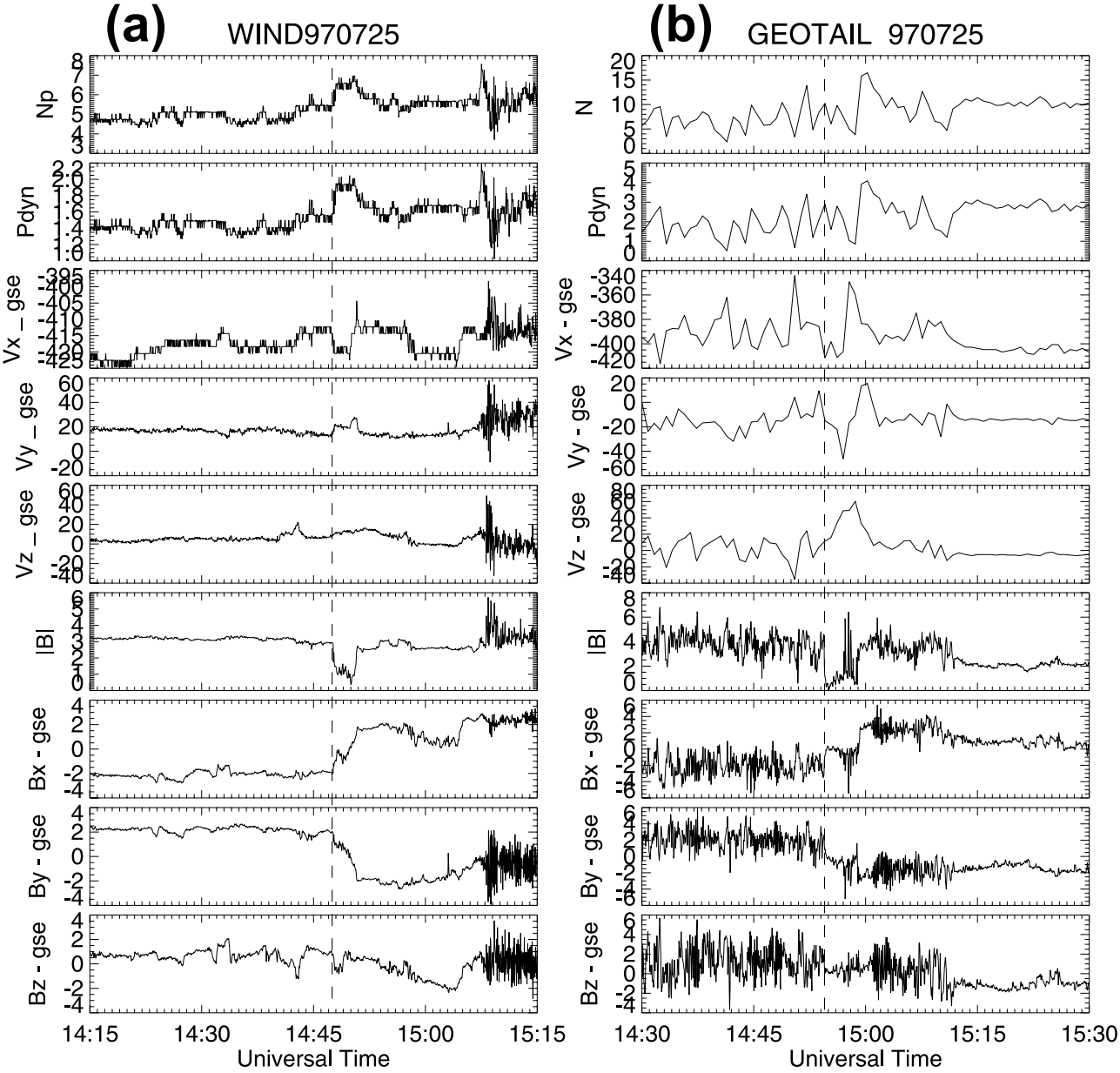

Figure 4. The solar wind plasma and IMF observations during the 1500 UT TCV at (a) Wind, (b) Geotail, (c) Interball, and (d) IMP 8.

wind flux), whereas the other four sensors lie on a plane perpendicular to the Sun-Earth line and spin with the spacecraft. The VDP data for 25 July 1997 shown in Figure 4c are at ~30 s time resolution. The remaining four panels in Figure 4c show the magnetic field magnitude and its x, y, and z GSE components. The magnetic field data are from the MIF-M fluxgate magnetometer, which is part of the ASPI experiment complex [*Klimov et al.*, 1997] and data are at 1 s resolution. The onset of the discontinuity at Interball is at 1459:30 UT, as shown by the vertical dashed line. The IMF strength at Interball decreases and the magnetic field rotates in the XY plane. There is weak evidence for an increase in the flux shown by the VDP0 sensor. The three perpendicular VDP sensors show a signature which is due to a very small flux of energetic electrons and not a signature of solar wind ion flux (J. Šafránková, personal communication, 2002). Interball therefore sees the same discontinuity but again there is evidence for spatial variations.

[13] Finally, Figure 4d shows the same solar wind and IMF properties as in Figures 4a and 4b from the IMP 8 spacecraft. The top five panels show solar wind properties from the Massachusetts Institute for Technology plasma instrument [*Lazarus and Paularena*, 1997] with a ~1 min time resolution (in practice, time resolution can be worse, with often missing data) and the bottom four panels show magnetic field data from the IMP 8 magnetometer (MAG) instrument [*King*, 1982] at 15.36 s time resolution. The onset of the discontinuity is at 1500:30 UT and it is determined by the IMF data because the time resolution of the plasma data is significantly lower (diamonds indicate individual data points). The magnetic field signature seen at IMP 8 is very similar to that observed at Interball (except

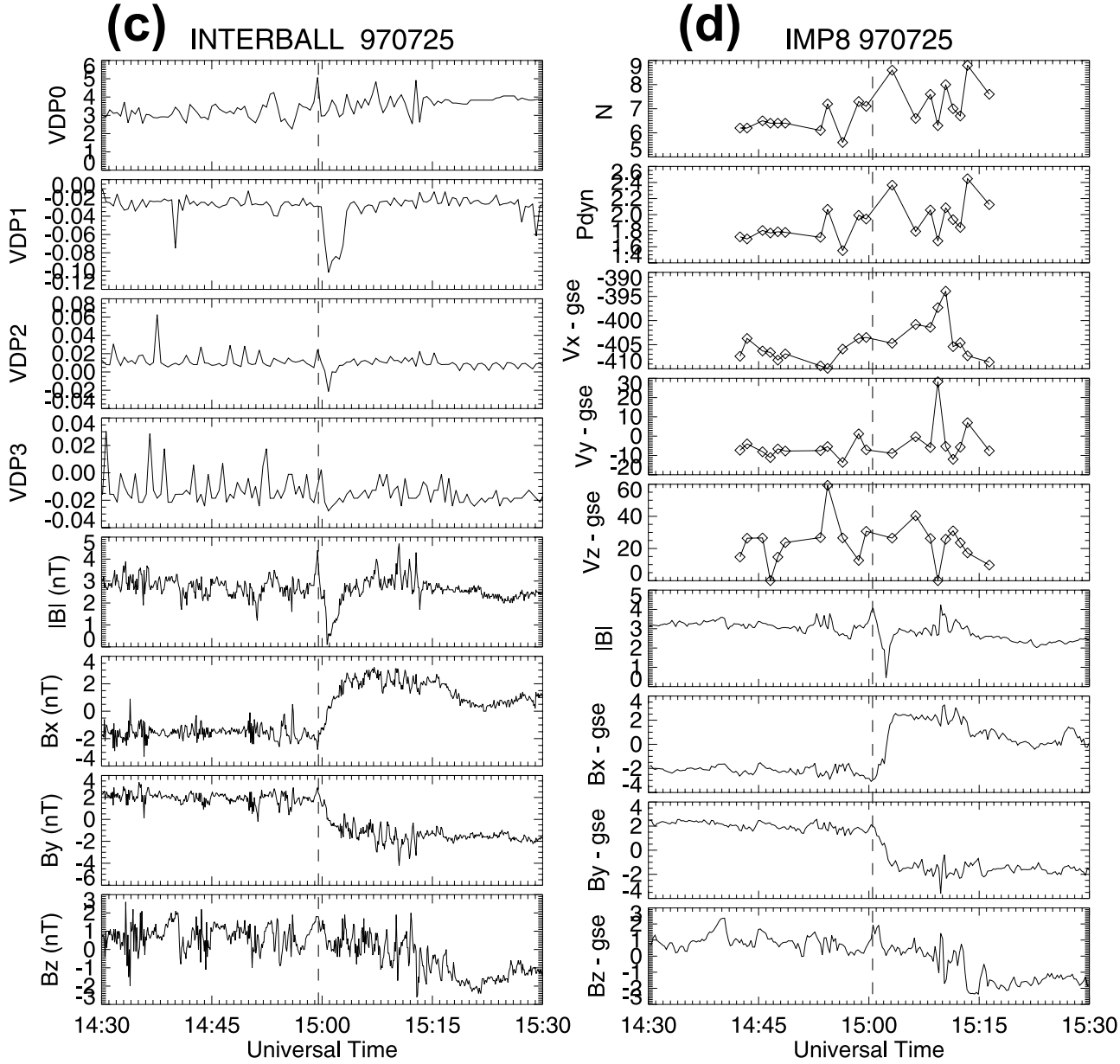

Figure 4. (continued)

IMP 8, being further away from the bow shock, does not observe the foreshock waves recorded by Interball during the time period plotted in Figure 4c). The IMF signature is accompanied by a small density enhancement at IMP 8 just as in Geotail and Wind.

[14] All four spacecraft therefore observe the same discontinuity. There is spatial variation in the discontinuity front but the main properties are maintained. This, along with the fact that the increase in density is accompanied by a decrease in the magnetic field, indicates that this is a well-organized MHD discontinuity and likely a tangential discontinuity (TD) (the total pressure remains constant across tangential discontinuities). To verify this assumption, we plot in Figure 5, from top to bottom, the dynamic pressure, the total pressure (as $3/2NkT + B^2/2\mu_0$), the plasma and magnetic pressures separately, the density, the temperature, and the magnitude of the magnetic field. It is clear that this discontinuity carries with it a dynamic pressure enhancement but the plasma and magnetic pressures across it vary in antiphase so that the total pressure is constant and the discontinuity is in thermal balance with the surrounding plasma. It therefore has all the characteristics of a TD, and we believe that it is a feature of the pristine solar wind that is advected and impacts the magnetopause. We believe that the dynamic pressure enhancement carried within this TD is responsible for triggering the ground TCV. Note that we could only use WIND to investigate the character of the trigger discontinuity because GEOTAIL signatures are affected by foreshock wave activity, Interball provides no ion plasma moments, and the plasma data from IMP 8 have too poor time resolution to produce meaningful results.

[15] In order to understand the creation (at the postnoon region) and propagation (westward) of the ground transient, we must understand where and how the TD front impacts the

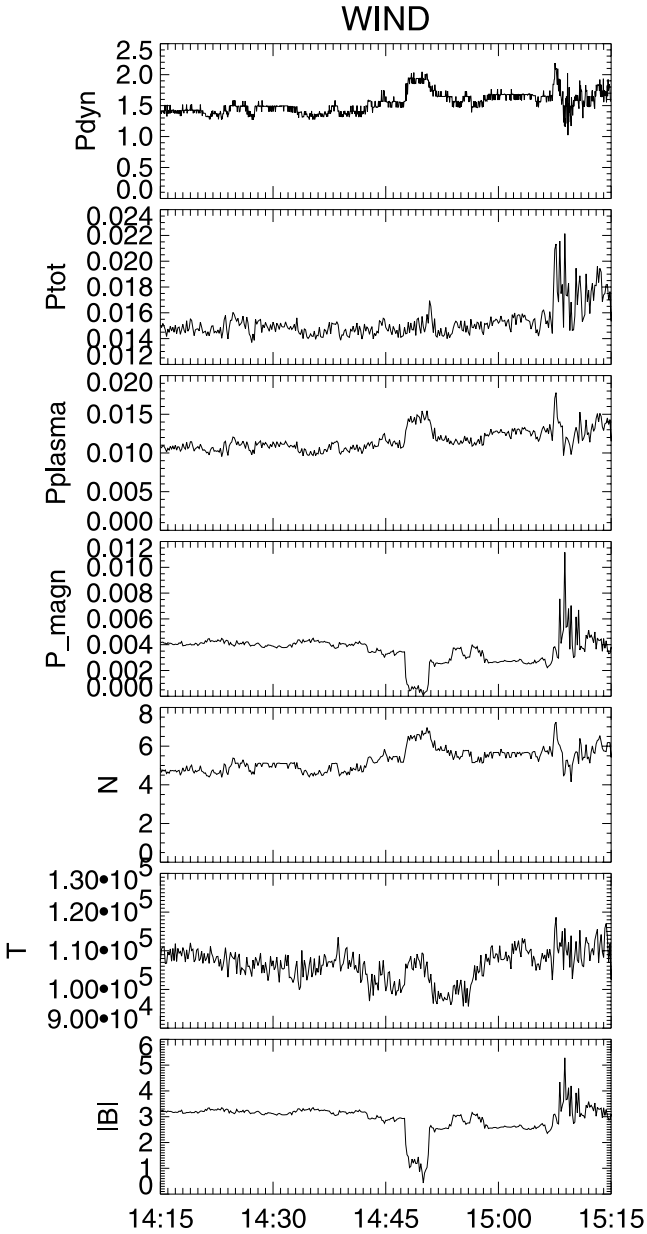

Figure 5. The different pressures during the 1500 UT discontinuity at Wind. From top to bottom are the dynamic, total, plasma, and magnetic pressures, respectively, the density, temperature, and magnetic field magnitude. The variations at ~1450 UT are due to a tangential discontinuity.

magnetopause. We do that by determining the orientation of the discontinuity boundary at the location of each spacecraft. We used minimum variance analysis [*Siscoe et al.*, 1968] and determined the unit vector normal to the front for which the normal component of the magnetic field has its minimum value. This method is particularly well suited for discontinuities for which the normal magnetic field is zero, as in a tangential (TD) or rotational (RD) discontinuity. Since the present discontinuity is a TD (Figure 5), the *Siscoe et al.* [1968] method is reliable. The GSE coordinates of the boundary normal unit vectors and the time periods we used to determine them are shown in Table 1. The ratio of the eigenvalues for the intermediate to minimum variance directions is the parameter λ and it indicates the confidence in the unit vector determination (the higher the λ, the better the unit vector determination). Figure 6 shows the projections of the determined discontinuity fronts and their normal unit vectors in the XY and XZ planes in GSE coordinates. The solid thick lines indicate the front orientation at the location of each spacecraft and the vectors are the normal unit vectors. All normal unit vectors are plotted in the same scale with the full unit length shown on the top right of Figure 6a. The length of the vectors plotted is proportional to the relative magnitude of the projection of the unit vectors on the XY and XZ planes. For example, it is clear from looking at the length of the vectors in Figures 6a and 6b that normals lie closer to the XY plane. For Wind and Geotail, two fronts have been determined and plotted in Figure 6. As mentioned above, when we were describing Figures 4a and 4b, Wind and Geotail observe the IMF rotation of the TD in two steps; we therefore determined a front for each step. The fronts for the first step are indicated with the solid thick lines and the fronts for the second step are indicated with a dashed line for Geotail and a dotted line for Wind. Note that the orientations of the first and second fronts are similar in the XY plane but that there is evidence for a significant rotation in the XZ plane. In the XY plane the front (the four thick solid lines) has an orientation aligned with the Parker spiral direction (which we will call "spiral orientation" in the remaining of this paper), which explains well the observed propagation of the front from Wind (at 1447:30 UT) to Geotail (at 1454:30 UT) to Interball (at 1459:30 UT) and finally to IMP 8 (at 1500:30 UT). Note, also, that in the XZ plane the TD front is basically vertical, except at the location of Interball. This is likely due to poor determination of the front orientation in the XZ plane because of the large amplitude foreshock waves and the absence of a TD signature in the Z-component of the magnetic field of the Interball observations (Figure 4c).

[16] We further strengthen our quantitative determination of the discontinuity front orientation and more accurately track its propagation between the four spacecraft and on the magnetopause by accurately determining and then predicting the time delays of the TD front arrival at the four spacecraft. We do this in three different ways: (1) from visual determination of the discontinuity onset from the IMF and plasma data (these are the times that we used above and indicated in our description of Figure 4), (2) from cross correlations of the discontinuity IMF disturbances between two spacecraft, and (3) predicting arrival times using the determined front orientation and the measured solar wind velocity.

[17] The first method could be argued to be the more accurate (albeit subjective) because there is a clear onset (to

Table 1. Boundary Normal Unit Vectors for the 1500 UT Discontinuity

Spacecraft	Times, UT	n_x, unit vect.	n_y, unit vect.	n_z, unit vect.	λ
WIND	1447–1448	0.711	0.702	−0.049	14.87
	1450–1451	0.432	0.555	0.710	13.7
GEOTAIL	1454–1455	0.637	0.767	0.075	5.97
	1459–1500	0.619	0.500	0.605	6.87
IMP 8	1500–1504	0.515	0.857	−0.006	12.6
INTERBALL	1500–1503	0.446	0.735	−0.511	6.05

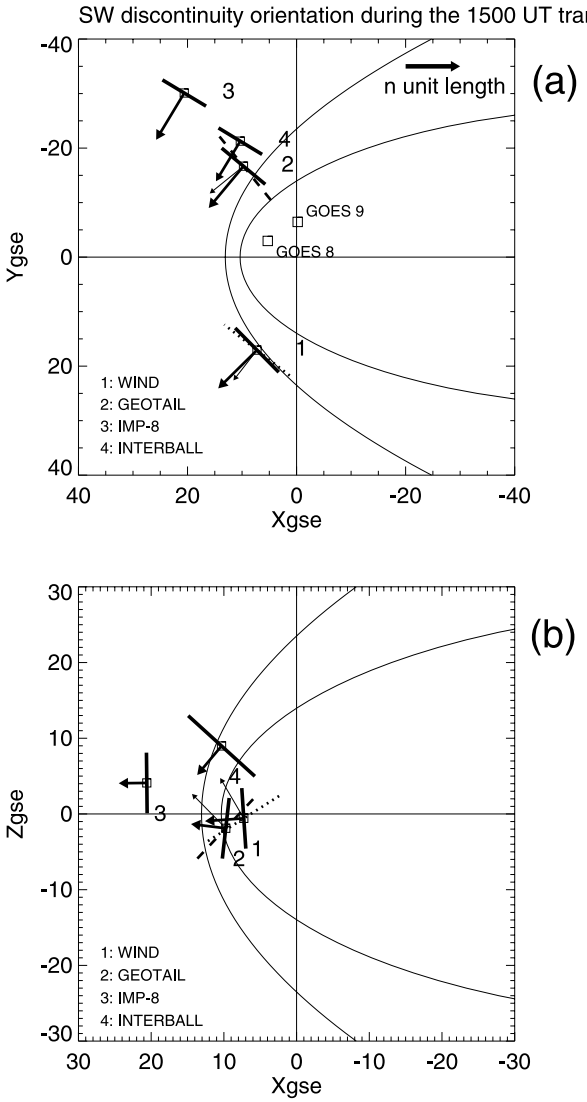

Figure 6. The projections of the determined discontinuity fronts during the 1500 UT event and their normal unit vectors in the XY and XZ planes in GSE coordinates. The solid thick lines indicate the front orientation at the location of each spacecraft and the vectors are the normal unit vectors. All normal unit vectors are plotted in the same scale with the full unit length shown on the top right of Figure 6a. The length of the vectors plotted is proportional to the relative magnitude of the projection of the unit vectors on the XY and XZ planes.

within half a minute) of the TD disturbances observed in at least one component of the IMF in all four spacecraft (see Figure 4). The cross correlation method can be an accurate and quantitative method that correlates the whole shape and pattern of the discontinuity (not just its onset) between spacecraft. The time delays determined from the onset of the discontinuity would be exactly the same as the ones determined from cross correlations if the shape of the discontinuity remained unchanged between spacecraft (which would imply no spatial variations of the discontinuity boundary). However, in this case the TD signatures differ some from spacecraft to spacecraft (for example between Geotail and IMP 8) and with the strong foreshock waves observed at Interball and Geotail we often got different results for different IMF components. We therefore used the average time delays determined from the cross correlation of the most relevant components (for example, for the WI-IT pair of spacecraft only |B|, Bx, and By were used in the cross correlation calculation because IT has no signature in the Bz component for this discontinuity; see Figure 4).

[18] The third and predictive method assumes planar fronts for the discontinuity propagating with the solar wind velocity. The time delay dt of the front propagating from spacecraft 1 to spacecraft 2 is based on the assumption that the orientation of the front as determined in the location of spacecraft 1 remains unchanged as it propagates to spacecraft 2. Then the time delay is given by the formula

$$dt(SC1 \rightarrow SC2) = \frac{\hat{n}_1 \cdot \mathbf{R}}{\hat{n}_1 \cdot \mathbf{V}_{SW}}, \quad (1)$$

where $\mathbf{R}$ is the vector distance between the two spacecraft, $\hat{n}_1$ is the normal unit vector of the TD front at the location of spacecraft 1, and $\mathbf{V}_{SW}$ is the solar wind velocity at the location of spacecraft 1. Equation (1) uses our knowledge of the front at spacecraft 1 and predicts when the front will arrive at spacecraft 2. If the determination of the front orientation is made reliably at spacecraft 1 and the propagation is planar and with a constant velocity then the predicted arrival time should compare well with the observed onset time of the discontinuity at spacecraft 2. This is another way to determine the discontinuity propagation characteristics and whether it has spatial variations at the distance between spacecraft.

[19] Table 2 shows the time delays, in seconds, determined by these three methods. Positive time delays indicate that the front propagates from spacecraft 1 to spacecraft 2 and negative delays indicate the opposite. The measured time delays are typically larger than the other two times, and they generally agree well with the cross correlation time delays to within 90 s or less. Any variations are due, we believe, to the changing shape and size of the discontinuity at the location of each spacecraft. Note also that the measured and cross correlation time delays indicate that the TD is seen first at Interball and then at IMP 8. However, the estimated time delay from Interball to IMP 8 is negative (sixth row in Table 2), indicating that IMP 8 should observe the TD first. This is clearly not what is happening (Figure 4). This discrepancy is again due to the rather ''poor'' determination of the TD front in the XZ plane at the location of Interball, as we discussed above. If we focus on the XY

Table 2. Time Delays Between Spacecraft During the 1500 Discontinuity

	dt, s		
Spacecraft SC1 → SC2	Measured	From Cross Correlations	Estimated From Equation (1)
WI → GT	420	362	489
WI → IT	720	661	564
WI → I8	780	782	534
GT → IT	300	204	57
GT → I8	360	277	71
IT → I8	60	49	−18
I8 → IT	−60	−49	−66

plane and assume that the TD front is vertical as seen in the other three spacecraft, then the relative location of the four spacecraft in the XY plane and the orientation of the front (see Figure 6a) explain well why Interball should indeed observe the TD before IMP 8. As a confirmation, we estimated in the last row of Table 1 the time delay from IMP8 to Interball (the front orientation is more accurately determined at IMP 8) and then all three methods accurately give very similar negative time delays, indicating propagation of the front from Interball to IMP 8.

[20] Figure 7 summarizes and demonstrates the propagation of the discontinuity in the solar wind and its effects in the magnetosphere. It shows a representative sample of key properties observed at the four solar wind monitors and the two geosynchronous GOES 8 and 9 spacecraft as well as on the ground, during the 1500 UT TCV event. The fourth and fifth panels show the dynamic pressure and magnetic field strength at WIND, where the character of the tangential discontinuity is more clearly observed. The onset of the discontinuity is first observed at WIND, due to its location in the afternoon sector, and then, as the TD propagates to the morning sector, it is observed by the other spacecraft as well. The orientation and propagation of the TD front explains well the generation and propagation of the transient on the ground (Figure 2) and in the magnetosphere (GOES data). Owing to its spiral orientation the TD front will first impact the magnetopause in the postnoon region, thus the ground transient is first created in the early afternoon hours. The TD front then propagates toward the morning region at the magnetopause, while it is advected antisunward with the solar wind. This explains the westward propagation of the ground TCV, first toward noon and then toward dawn (once it has gone past local noon). This is also evidenced by the propagation of the compression (indicated with arrows in Figure 7) from GOES 8 to GOES 9. It is difficult to determine the onset of the compression at GOES with accuracy. However, we determined, by visual inspection, the time that the magnetic field component Hp begins to grow above the background trend as the possible onset time of the compression at each spacecraft. Thus possible onset times are at 1449:00 UT at GOES 8 and at 1451:00 UT at GOES 9. Comparing these times with the onsets of the discontinuity at the four solar wind spacecraft, we see that GOES 8 and 9 observe the compression after the onset of the TD at Wind and before the onset at Geotail. This is in perfect agreement with our determination of the propagation orientation of the TD front shown in Figure 6a.

[21] The B_x component at the ground station of Rankin Inlet is plotted on the top panel of Figure 7, and it shows a signature well correlated with the GOES compressional signatures. Our conclusion is that the dynamic pressure enhancement that was carried by the TD (a feature of the pristine solar wind) triggered the ground TCV and the propagation characteristics of the TD determined the propagation of the transient in the magnetosphere and ionosphere.

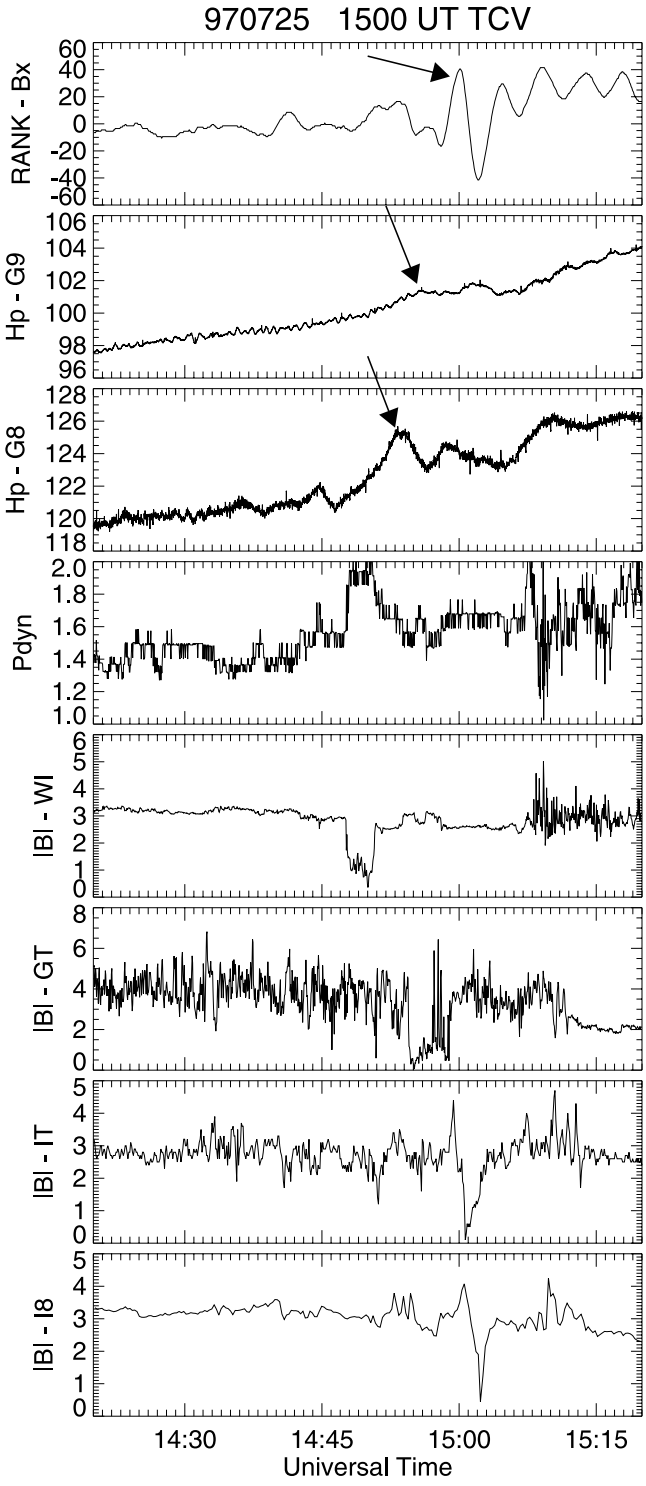

Figure 7. Summary of various properties indicating the propagation of the tangential discontinuity that triggered the 1500 UT TCV.

3. The 1830 UT Discontinuity: Trigger of the Second Ground Transient

3.1. Transient on the Ground

[22] Figure 8 shows the ground magnetometer signature of the second transient on 25 July 1997. The figure has the same format as Figure 2, i.e., it plots the data of a representative set of magnetometer stations that are aligned along the ~73°–74° magnetic latitude and covering 10 hours in MLT. The MLT of each station at 1830 UT is noted over each station trace in Figure 2. The onset of the transient is at ~1834 UT, and it appears first in the westernmost stations (CONT and BL) located near

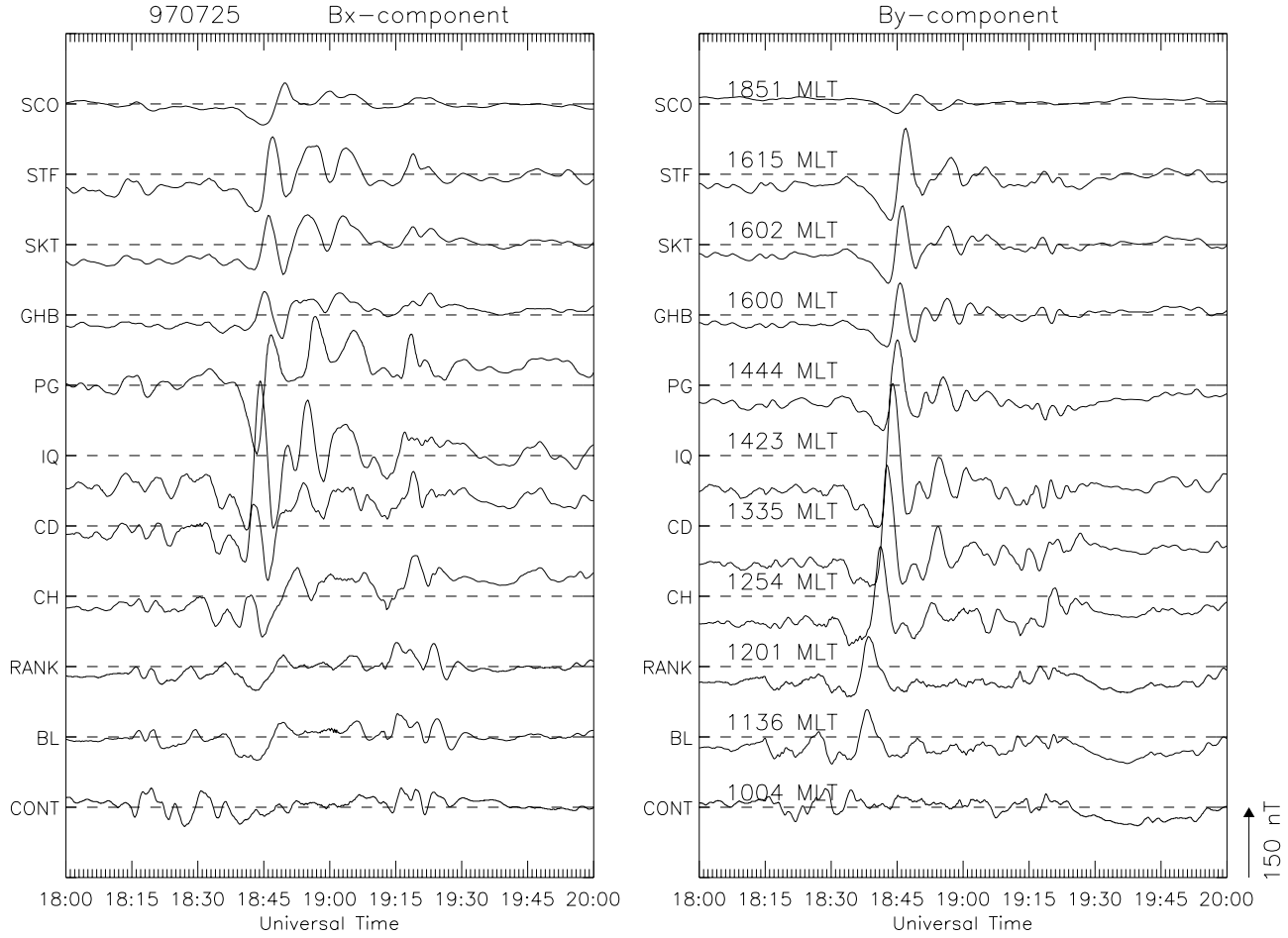

Figure 8. The ground magnetometer signatures of the 1835 UT TCV. The same set of magnetometers is plotted as in Figure 2.

1200 MLT and then propagates eastward toward the afternoon and evening sector. Most of the ground stations are in the afternoon sector, and only the western CANOPUS and MACCS stations are in the prenoon and noon region. The transient reaches peak amplitude of ~300 nT in the 1300–1400 MLT sector, and it weakens as it continues propagating eastward toward later MLTs (it is ~150 nT at 1800 MLT). Note that there are other transient perturbations in the two-hour period plotted in Figure 8, especially in the Bx component (some much weaker variations exist at ~1815 UT and at 1915–1930 UT), but the 1835 UT transient is the strongest and most coherent perturbation and exhibits a clear propagation pattern (not seen in the smaller perturbations).

[23] Analysis of the equivalent ionospheric currents (discussed in detail by *Murr et al.* [2002]) shows that the transient consists of a set of two eastward propagating vortices, with an upward field-aligned current at the center of the leading counterclockwise vortex and a downward field aligned current at the center of the trailing clockwise vortex. Therefore, this event is also a typical traveling convection vortex (TCV) event.

3.2. Solar Wind and IMF Data

[24] At the time of the second TCV event, Geotail, Interball, and IMP 8 were still in the solar wind at similar local times as for the first TCV event (Figure 3), but Wind has moved into the magnetosheath. Figure 9 shows the locations of the four solar wind spacecraft and of GOES 8 and 9 in the XY and XZ GSE planes. Again the location of the magnetopause and bow shock were determined based on the *Roelof and Sibeck* [1993] and *Fairfield* [1971] results, respectively. Figure 10 shows the solar wind plasma and IMF observations at (a) Interball, (b) IMP 8, (c) Geotail, and (d) Wind during the 1835 UT TCV event. The same properties from each spacecraft are plotted here as in Figure 4. The 1800–2000 UT period is plotted for all four spacecraft, and the discontinuity we believe responsible for the ground TCV is indicated with the darkest shading. The four time periods with the lighter shading in the four plots of Figure 10 indicate four other discontinuities of the 2 hour period plotted, which we will examine in a later section and which did not produce significant ground transients.

[25] The onset of the trigger discontinuity is at 1828:30 UT at Interball, at 1833:00 UT at IMP 8, at 1842:00 UT at Geotail, and at 1847:30 UT at WIND. The discontinuity has a leading and a trailing edge, and it exhibits increases in the magnitude of the magnetic field, increases in the B_x and B_y and a decrease in the B_z component, and a small increase in the density and dynamic pressure. The perturbations and their duration have significant variation from one spacecraft to the next indicating significant and small-scale (~few R_E)

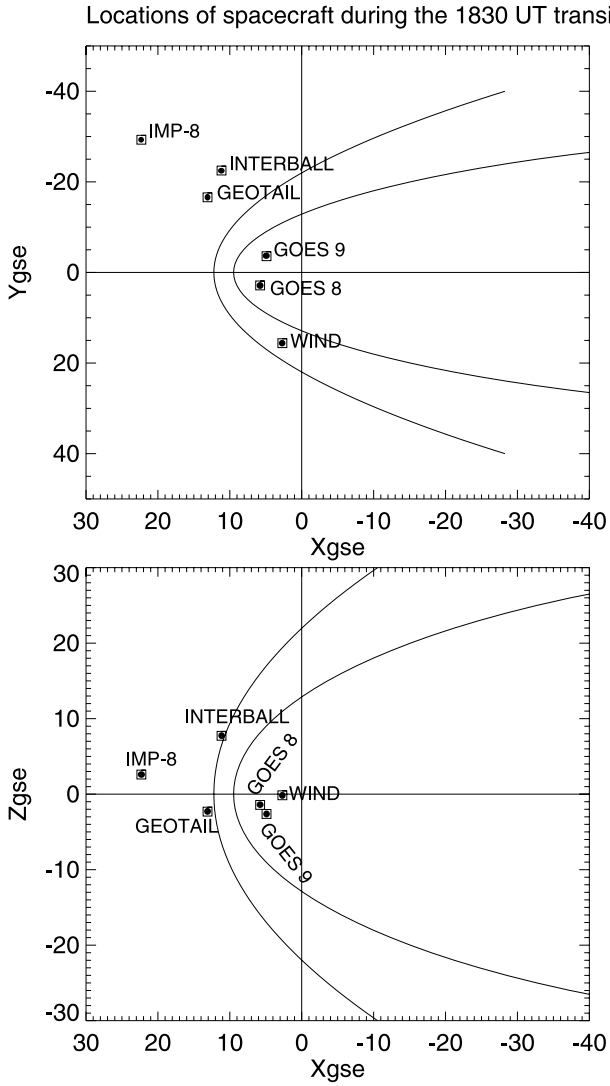

Figure 9. The locations of the four solar wind monitors and the two GOES spacecraft during the 1835 UT TCV.

spatial structure of the discontinuity region in the solar wind. We have determined the onset of the discontinuity by visual inspection of the most clear perturbation signatures at each spacecraft. Our visual determination shows the solar wind structure propagating from Interball to IMP 8, then to Geotail, and finally to WIND. By observing the relative separation of the spacecraft in the Zgse direction in Figure 9, such propagation is possible if the normal to the discontinuity front has a significant component in the Zgse direction (we will see below that this is likely the case). We must caution, however, to the fact that our visual determination of the discontinuity onset at Interball may have a significant degree of uncertainty as the signature of the structure is not sharply defined (see below Figure 10a). Therefore it is not certain whether IMP 8 or Interball observe the onset first.

[26] At Interball (Figure 10a) the signature is the least well defined, and it shows as an increase in the antisunward flux (VDP0), in $|B|$, and B_x, but no signature is detected in the B_y and B_z components. The discontinuity has a clear leading edge but no clear trailing edge, and just before its arrival Interball observes strong waves (probably associated with the foreshock region) that significantly reduce in amplitude (especially in the B_z component) after the arrival of the discontinuity.

[27] At IMP 8 (Figure 10b) there is no clear signature in the $|B|$ and B_x; instead the B_y and B_z perturbations are more clear. Variations observed at IMP 8 have a clear leading edge and a trailing edge (at ~1845:00 UT). Perturbations in the plasma data are not as pronounced; however, there seems to be a small enhancement both in the density and in the solar wind velocity bound by equally small and short-lived (a couple of minutes) decreases. Since both the magnetic field and the density increase in phase, the total pressure is not conserved across the discontinuity, and therefore this cannot be a tangential discontinuity. For verification we plotted the same properties as in Figure 5 (plot not shown in the paper), and it was clear that the total pressure is not maintained across this discontinuity. In fact this discontinuity does not have the properties of any standard MHD discontinuity.

[28] At Geotail (Figure 10c) variations are observed in all the magnetic field components as well as in the plasma data (density, velocity, dynamic pressure). The sharpest changes are in the IMF B_y and B_z components, just as at IMP 8, and the plasma data indicate a small increase in the dynamic pressure, in agreement with IMP 8. There are large-amplitude, short-period waves surrounding the discontinuity, implying that Geotail is in the foreshock region. There are many similarities in the discontinuity signatures between IMP 8 and Geotail, but the variations observed by Geotail are sharper and shorter in duration, implying a smaller-scale or faster discontinuity. Notice that there is similarity in the perturbations between Interball and IMP 8, and between IMP 8 and Geotail, but there is much less similarity between Interball and Geotail.

[29] At WIND (Figure 10d) the arrival of the discontinuity is marked by a brief entry into the magnetosphere (it exits into the sheath again on the trailing edge of the discontinuity). This is evidenced by the significantly decreased density, highly disturbed velocities, and the strong northward magnetospheric magnetic fields. In short, the discontinuity carries with it, inside the magnetosheath, a dynamic pressure decrease so that the magnetopause boundary locally expands outward. This is the opposite of the small pressure enhancement that is observed by both IMP 8 and Geotail in the upstream region. This is the first indication that perhaps this discontinuity strongly interacts with the bow shock thus creating the perturbation (possibly a hot flow anomaly (HFA) or a foreshock cavity) that eventually triggers the transient. There is low correlation in signatures between Geotail in the morning foreshock and WIND in the late afternoon sheath; therefore there is a degree of uncertainty in the association of the discontinuity features between WIND and the other spacecraft. However, even though our analysis for this discontinuity cannot be conclusive, we believe our interpretation is the most likely, as it fully explains the observations in the magnetosphere and ionosphere. Thus we believe that the brief entrance of WIND inside the magnetosphere is indeed associated with the passage of the same discontinuity because the duration of the magnetosphere entrance is similar to that of the discontinuity and because there is no other discontinuity for ~30 min before and after

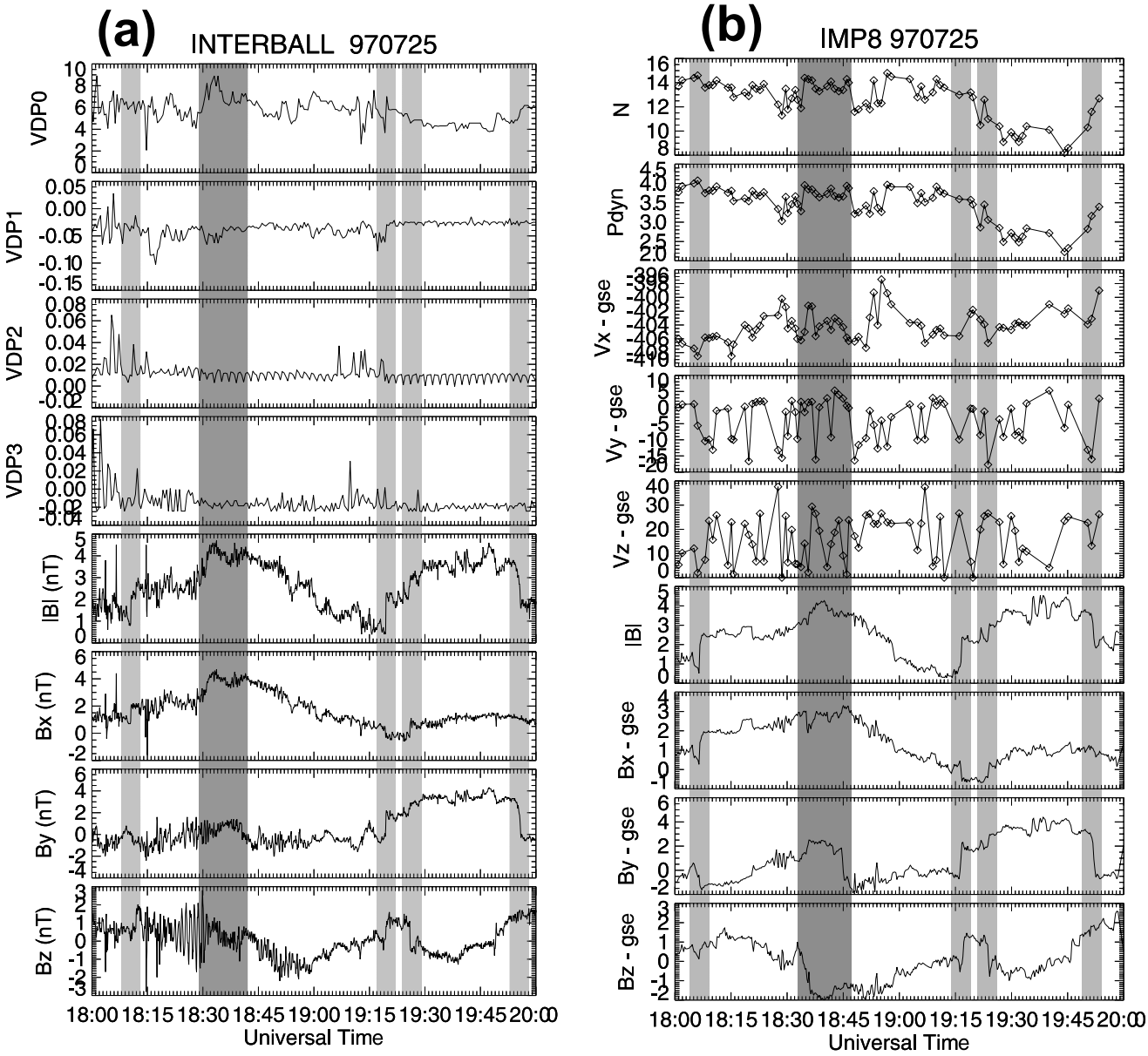

Figure 10. The solar wind plasma and IMF observations during the 1835 UT TCV at (a) Interball, (b) IMP 8, (c) Geotail, and (d) Wind.

that can be identified as the reason for the brief entrance of WIND in the magnetosphere.

[30] We again used minimum variance analysis to quantitatively determine the orientation of the discontinuity fronts at the location of each spacecraft, except at Wind, which is in the sheath and magnetosphere during the discontinuity. The leading and trailing edges of this solar wind structure imply two separate discontinuities bounding it. We determined the orientation for both the leading and trailing edge, when observed. The GSE coordinates of the boundary normal unit vectors and the time periods we used to determine them are shown in Table 3. The values of the parameter λ reported in Table 3 indicate that the unit vectors are reasonably well defined for IMP 8 and Geotail but poorly defined for Interball. This is not surprising considering the less sharply defined signatures of the discontinuity at Interball as we discussed above.

[31] Figure 11 shows the projections of the determined planes and their normal unit vectors in the XY and XZ planes. The thick solid lines and thick arrows indicate the orientation of the leading edge and its unit vector, while the dashed lines and thinner vectors indicate the orientation of the trailing edge. Again the lengths of all the normal vectors are plotted on the same scale as in Figure 6. Observe that the projected normal vectors are stronger in the XZ plane both for the leading and trailing edge of the solar wind structure. This simply means that the projection on the XZ plane is the more relevant one when trying to determine the timing of the observed signatures between spacecraft as the discontinuity propagates. The XZ projection (Figure 11b) indicates that Interball should observe the discontinuity first, then IMP 8, and finally Geotail, which is in agreement with our observations (Figure 10). We discussed above our lack of confidence in the accurate determination of the timing

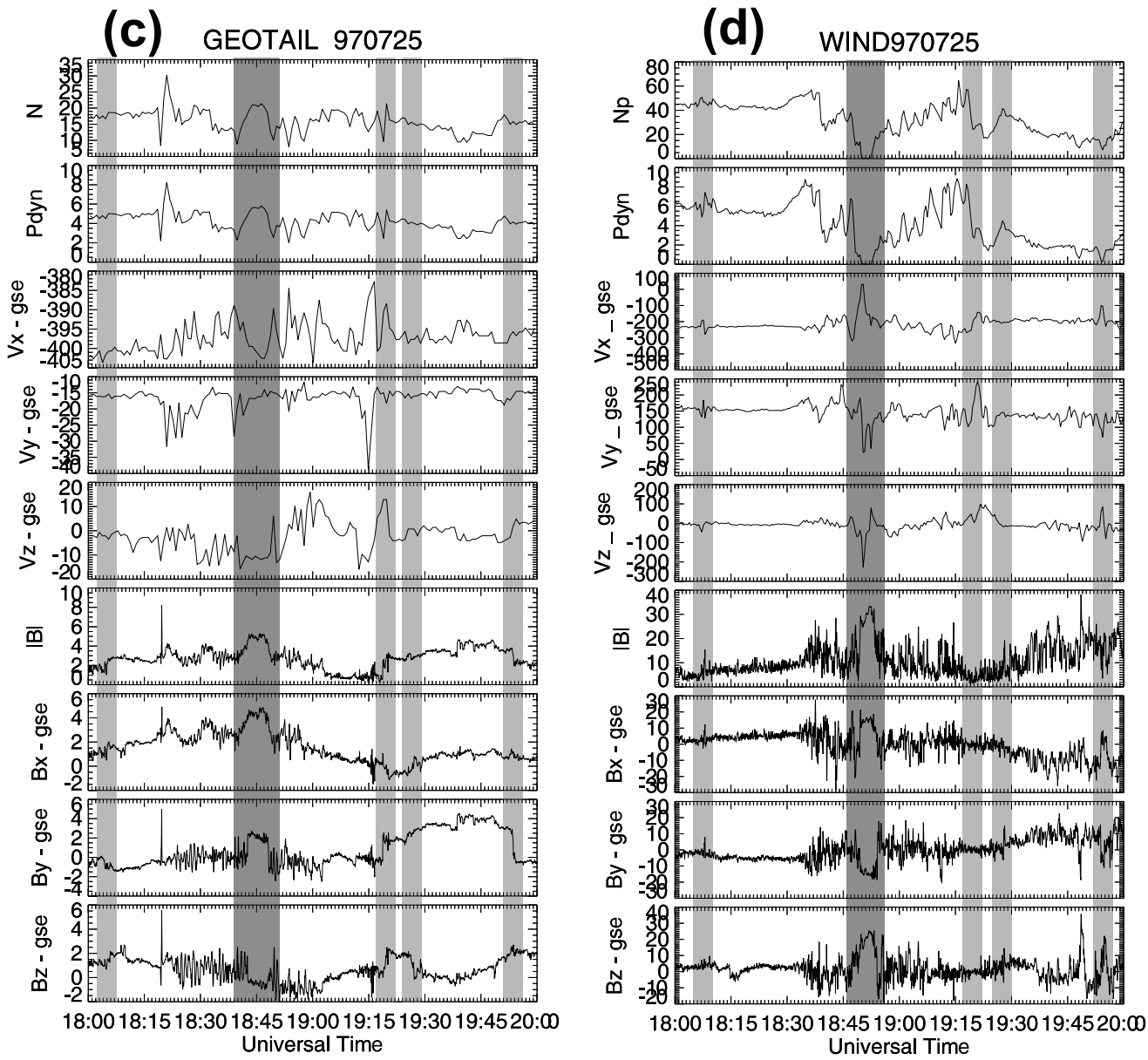

Figure 10. (continued)

between the spacecraft, and we are confronted with the same issue of limitations in our analysis here again. The minimum variance analysis we employed [*Siscoe et al.*, 1968] for the determination of the boundary normal unit vector is better suited for a tangential or rotational discontinuity. However, the observed discontinuity in the solar wind is not a tangential discontinuity. We also applied the *Sonnerup and Cahill* [1967] method of minimum variance analysis, which is less restrained and appropriate for a more general type of discontinuity; however, the results were not physically meaningful. The determined discontinuity boundary was such that most of the magnetic field was normal to that boundary, which is not physically meaningful for solar wind discontinuities. We are thus using the results of the *Siscoe et al.* [1968] method, and note the limitations that are thus imposed on our interpretation of those results, namely, that the fronts plotted in Figure 11 could have a large degree of error. In summary, we believe that the determination of the large Z-component of the front normal unit vector is accurate and partly explains the propagation pattern of the discontinuity, but the exact timing between spacecraft cannot be determined accurately due to significant spatial structure of this discontinuity.

[32] The observed and predicted (from equation (1)) time delays of the discontinuity arrival at the three spacecraft are

Table 3. Boundary Normal Unit Vectors for the 1830 UT Discontinuity

Spacecraft	Times, UT	n_x, unit vect.	n_y, unit vect.	n_z, unit vect.	λ
INTERBALL	1831–1833	0.176	−0.027	−0.984	1.32
	1839–1841	Not clear	Not clear	Not clear	–
IMP 8	1834–1836	0.334	−0.710	−0.620	27.26
	1844–1846	0.367	0.146	0.919	813.9
GEOTAIL	1842–1843	0.281	−0.601	−0.748	16.4
	1847:30–1848:30	0.009	−0.125	0.996	47.3

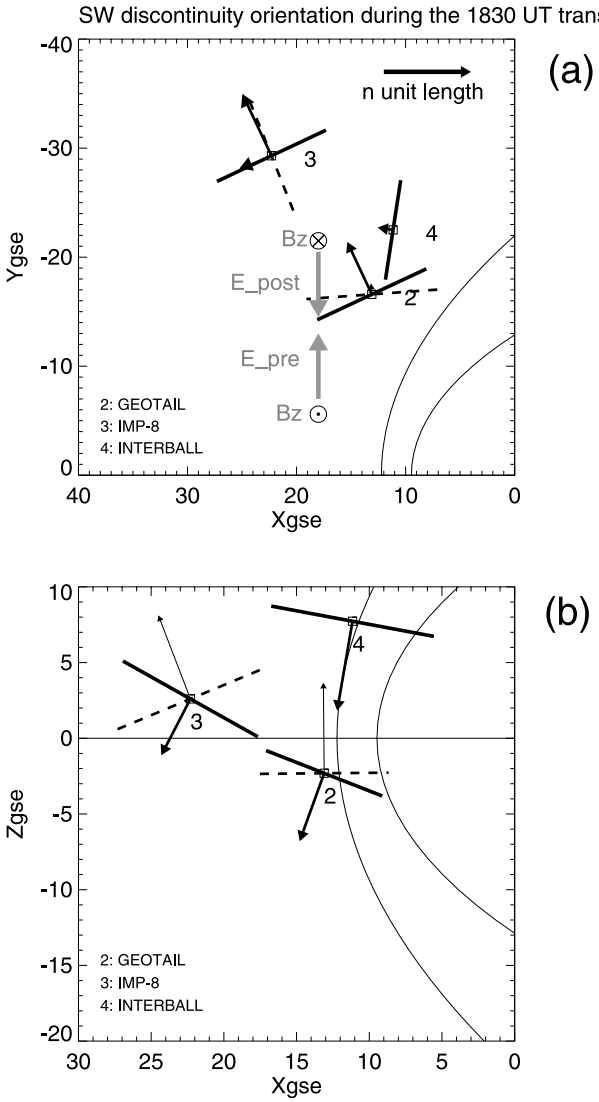

Figure 11. The projections of the determined discontinuity fronts during the 1835 UT event and their normal unit vectors in the XY and XZ planes in GSE coordinates. All normal unit vectors are plotted in the same scale with the full unit length shown on the top right of Figure 11a.

shown in Table 4. The predicted time delays are in the opposite direction from the measured time delays. This again is not surprising, based on our discussion above, and it only intensifies the conclusion that the determination of the boundary normals is only a qualitative one. Also, note that we have not included here time delays determined from cross correlation as we did in Table 2. The overall pattern of the observed discontinuity is so obviously different from one spacecraft to the next that such a calculation is not meaningful.

[33] Figure 12 presents a representative sample of key properties of the discontinuity observed at the four solar wind monitors, the two GOES spacecraft, and of the response at the ground station of Iqaluit. The total flux from the sunward sensor, VDP0, at INTERBALL is plotted in the fourth from the top panel, and the B_x (dashed) and B_z (solid line) components of the magnetic field are plotted in the fifth panel. The discontinuity is soon after observed inside the magnetosphere and on the ground and it also propagates to IMP 8 and then to Geotail and Wind (the gray vertical bars on the time axis of each IMF panel indicate the onset of the discontinuity at the spacecraft). Propagation in the magnetosphere is from GOES 9 to GOES 8, i.e., eastward just as on the ground (Figure 8). Also note that the differences of the signatures at the four solar wind monitors in Figure 12 indicate the significant and small-scale spatial structure of the discontinuity.

[34] The main perturbation at GOES 9 and 8 is a depression of the field in agreement with the outward expansion of the magnetopause at WIND (last panel) and with our suggestion that a foreshock cavity or HFA was created by the interaction of the discontinuity with the bow shock that subsequently triggered the strong magnetospheric and ground transient. We discuss this further in the next section. The minimum of the depression is observed at 1842:30 UT at GOES 8 and at 1838:30 UT at GOES 9. We determined, by visual inspection, the possible onset of the field depression at each spacecraft. The onsets are at 1833:00 UT at GOES 9 and at 1838:30 UT at GOES 8. GOES 9 observes the depression after the onset at Interball, at the same time with the onset at IMP 8 and before the onset at Geotail and Wind. Our suggested scenario for that event then is that the discontinuity hits Interball (the furthest away from the ecliptic plane) while a cavity is created at the same local time at the bow shock. The depression associated with the cavity quickly travels through the magnetosheath and impacts the magnetopause and soon after it is seen by GOES 9 at the same time that the discontinuity front has traveled along Z and closer to the ecliptic plane and impacted IMP 8. At the same time the HFA is traveling eastward and so does the depression at the magnetopause and in the magnetosphere. Geotail located closer to noon and at lower Z distances observes the discontinuity even later and Wind, located in the late afternoon sheath, sees it last as a magnetopause expansion.

3.3. Candidate for a HFA or a Foreshock Cavity

[35] Hot flow anomalies (HFA) are disturbances observed very near the bow shock and result from the interaction of an interplanetary current sheet with the bow shock. Usually, the current sheet is a tangential discontinuity, but that is not a necessary condition. The observed characteristics of HFA include central regions with hot, tenuous plasma with greatly disturbed magnetic fields and deflected flow velocities and duration of a few minutes [see *Schwartz et al.*, 2000, and references therein]. Prior studies have shown that for such a disturbance to be created the following conditions must be satisfied: (1) the solar wind convection electric field (and thus the solar wind flow) must be pointing toward and at a large angle with the current sheet on at least one side of

Table 4. Time Delays Between Spacecraft for the 1830 UT Discontinuity

Spacecraft SC1 → SC2	dt, s Measured	dt, s Estimated From Equation (1)
IT → I8	270	−846
I8 → GT	540	−130
IT → GT	810	−1410

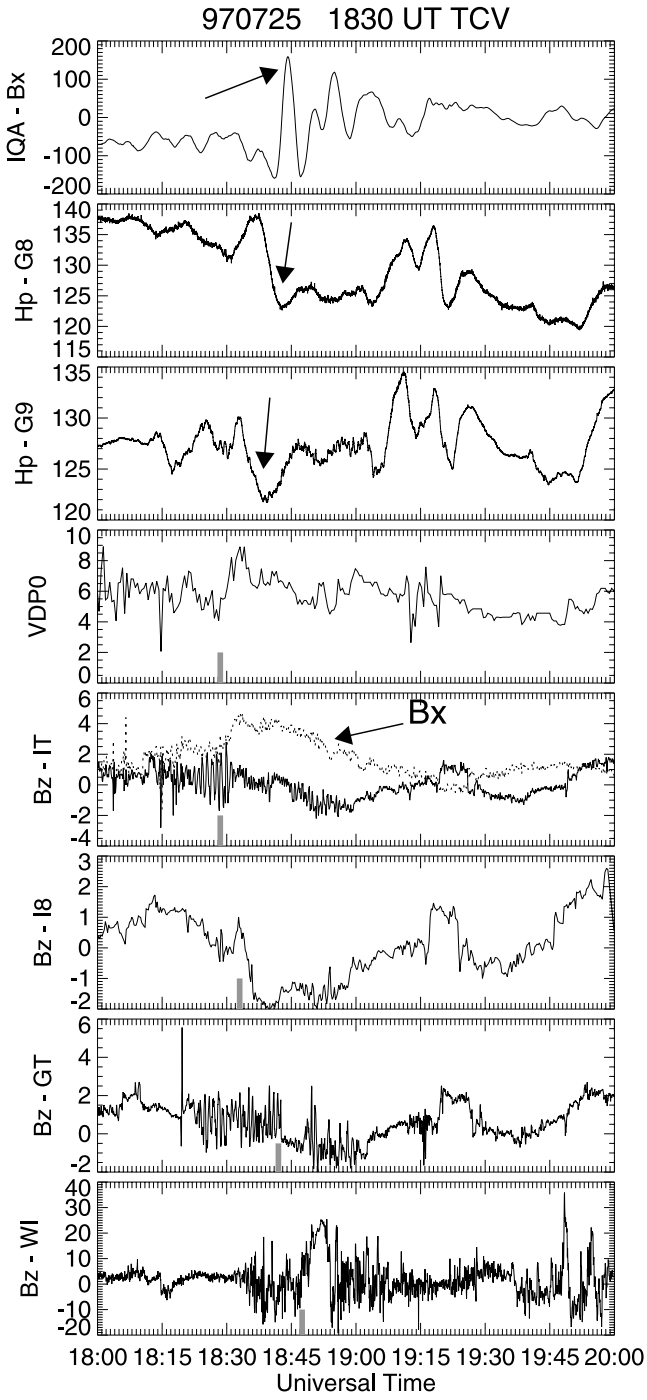

Figure 12. Summary of various properties indicating the propagation of the discontinuity that triggered the 1835 UT TCV. Short gray vertical bars on the time axis of each IMF panel indicate the onset of the discontinuity at that spacecraft.

the current sheet, and (2) the current sheet should pass relatively slowly along the bow shock, which means that the normal to the sheet should lie nearly perpendicular to the X-axis (or otherwise have a large cone angle).

[36] During our event none of the three spacecraft in the solar wind observe the clear HFA properties described by *Schwartz et al.* [2000]. For example, Geotail and IMP 8 do observe the higher temperatures (not shown) expected with a HFA, but they also observe increased (as opposed to decreased) densities and magnetic field (Figures 10b and 10c). In addition, no deflected flows are observed at Interball (no flux at VDP1, 2, and 3 in Figure 10a), IMP8, and Geotail (no V_y and V_z perturbations). It is possible that a HFA never developed at the bow shock or that it did not develop sufficiently to have the depressed magnetic field and deflected flows. It is also possible that Geotail and IMP 8 are not close enough to the bow shock to observe the actual excavated cavity of the HFA, if it indeed developed.

[37] Another possibility is that the interaction of the discontinuity with the bow shock results in a foreshock cavity instead of a HFA. Foreshock cavities are similar to HFAs in that they are created by hot backstreaming ions reflected at the bow shock on field lines connected to the bow shock. They are also characterized by higher temperatures (but not as high as in HFA) depressed magnetic fields, and density, but not by deflected flows [*Sibeck et al.*, 2002]. Foreshock cavities are much more common than HFAs, and for them to be created only the second of the two conditions described above needs to be satisfied, namely that the boundary normal should point transverse to the Sun-Earth line.

[38] We examine whether the two conditions described above are satisfied or not for the 1835 UT discontinuity.

[39] 1. We investigate the first condition at the location of Geotail, where the discontinuity signature is the most clear. The solar wind convection electric field before and after the discontinuity is due primarily to the IMF B_z component ($B_y \cong 0$ during the same time, and B_x does not contribute to the convection electric field, see Figure 10c). The convection electric field before and after the front and the direction of Bz are shown in Figure 11a at the location of Geotail. The electric field points toward the plane of the discontinuity both before and after, so the first condition for a HFA creation is satisfied.

[40] 2. Figure 11a and 11b indicate that the second condition is also satisfied. Normals to the fronts lie nearly perpendicular to Sun-Earth line, implying long convection times across the dayside bow shock.

[41] Thus the conditions are favorable for the creation of a HFA by the interaction of the discontinuity with the bow shock.

4. Comparison With Other Discontinuities

[42] During the above analysis we were able to identify the solar wind triggers of the two TCVs observed on 25 July 1997. The trigger of the first TCV was a "well-behaved" tangential discontinuity, which carried a dynamic pressure enhancement with it. The trigger of the second TCV was a much more complicated discontinuity, with significant spatial structure that we believe generated either a hot flow anomaly or a foreshock cavity at the bow shock and a rarefaction in the magnetosheath that impacted the magnetosphere and triggered the ground transient. The IMF around the time of the second TCV is more disturbed, and there are a number of other discontinuities that do not however create significant transients on the ground. We analyzed all four other discontinuities in the 1800–2000 UT time period (around the second TCV) in an attempt to

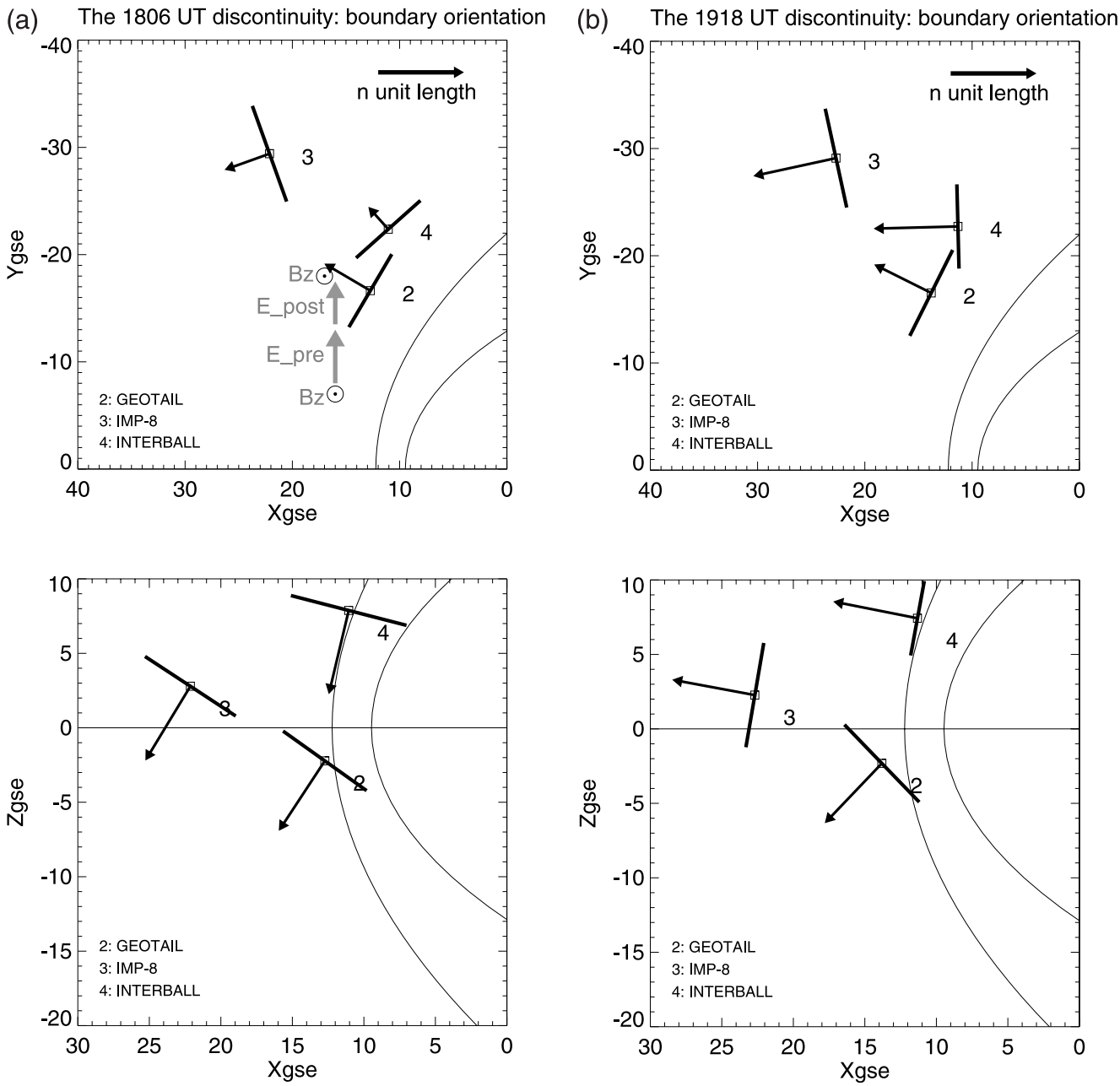

Figure 13. The determined discontinuity fronts for four other discontinuities used for comparison with the 1835 discontinuity: (a) the 1806 UT discontinuity, (b) the 1918 UT discontinuity, (c) the 1925 UT discontinuity, and (d) the 1950 UT discontinuity.

understand why these discontinuities did not trigger large TCVs. These four discontinuities are shown in Figure 10 under the four lighter shading areas in the plots of each spacecraft. We have determined the boundary normals at Geotail, IMP 8, and Interball in the solar wind. WIND is in the sheath during that period, and even though there are no clear correlations between the signatures in the sheath and in the solar wind we have attempted (with the lighter shading in Figure 10d) to identify the possible signature of each of the four discontinuities at WIND.

4.1. Discontinuity 1 at 1806 UT

[43] This discontinuity exhibits an increase in the magnetic field |B| and its B_x component and a smaller increase in the B_z component (not clear at all spacecraft). There are no clear plasma (velocity, density, temperature) perturbations associated with the discontinuity, and the total pressure (not shown) is not maintained across it. The discontinuity propagates from Geotail to IMP 8 and then to Interball. From Figure 8 we see that there is no perturbation in the ground magnetograms associated with this discontinuity; in fact there is no perturbation until 1815 UT.

[44] Figure 13a shows the orientation of the discontinuity fronts in the XY and XZ GSE planes. All normal vector projections are plotted on the same scale. The large Z component of the boundary normal unit vectors (in the XZ plane projection) and the plotted orientation explain the propagation of the discontinuity front between spacecraft.

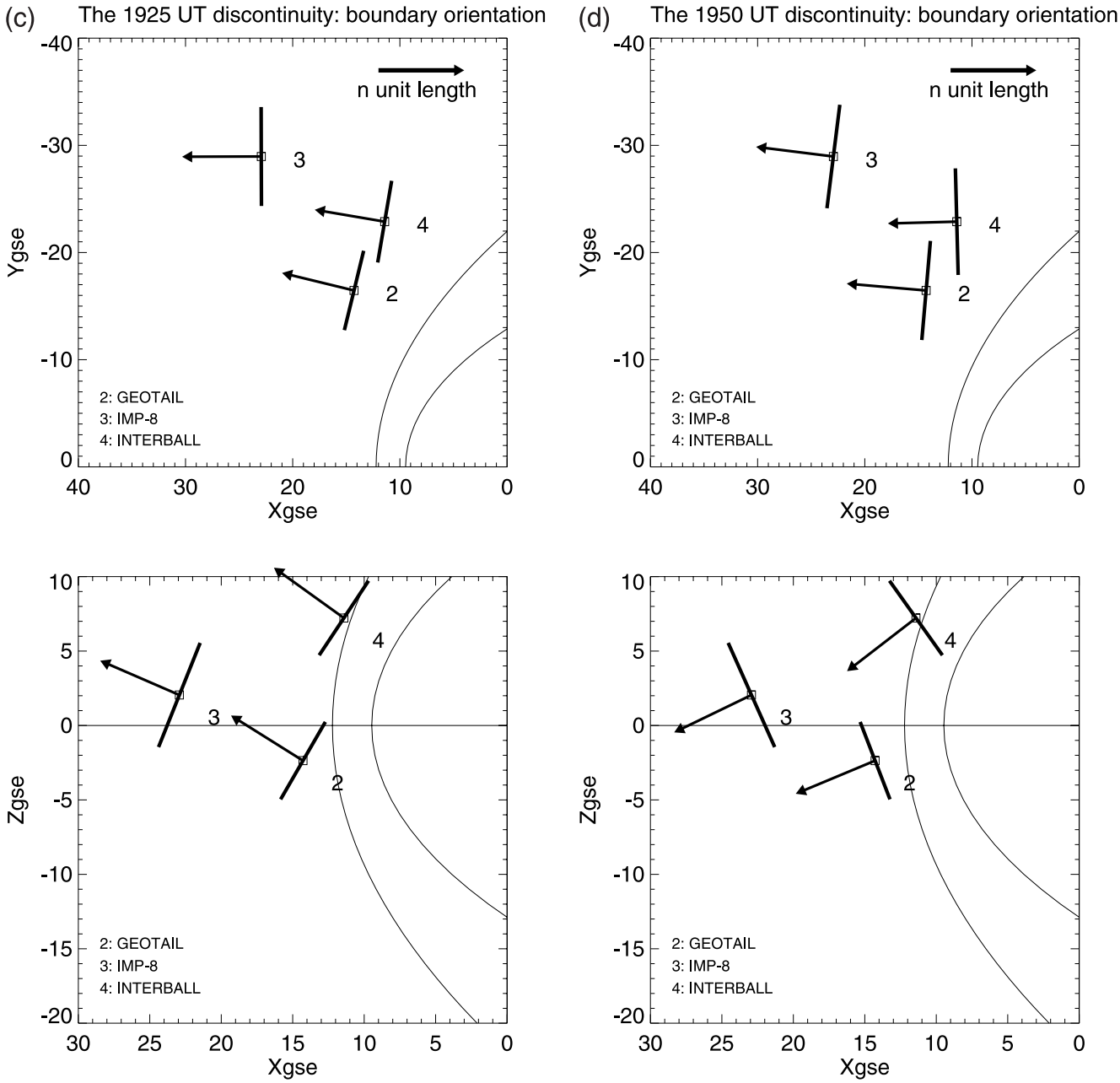

Figure 13. (continued)

We have estimated the time delays between the three spacecraft using equation (1), as we did for the trigger discontinuities of the two TCVs, but we do not show the results for brevity. The delay estimates are in good agreement with the measured delays, giving further confidence to our calculation of the front normal at each spacecraft.

[45] Since this discontinuity does not carry a dynamic pressure perturbation that could trigger a transient, the next step is to investigate whether it satisfies the two conditions described above in section 3.3 so that the trigger of the ground transient could be created by the interaction of the discontinuity with the bow shock. It appears from the XZ plane of Figure 13a that this discontinuity passes the large cone angle test. More precisely, the cone angle of the normal vector at Geotail is 58°. *Schwartz et al.* [2000] find that a current sheet whose normal vector has a cone angle larger then 60° is likely to create a HFA (specifically, current sheets normals with cone angles larger than 60° accounted for 80% of all HFAs in the work of Schwartz et al.). However, the discontinuity fails the converging electric field test because the convection electric field is in the same direction before and after the discontinuity and it is mostly parallel to the discontinuity plane rather than at a large angle to it (as shown in Figure 13a, in the XY plane at the location of Geotail and with the gray-colored vectors). This means that it is unlikely that this discontinuity will create a HFA at the bow shock and we would predict that no significant ground transient may be triggered, as, in fact, happens.

4.2. Discontinuity 2 at 1918 UT

[46] This discontinuity exhibits an increase in |B|, By, and Bz and a decrease in Bx. Geotail registers a sharp pulse in

density and Interball in the total flux, while no variation is seen in the IMP 8 plasma data. WIND observes a significant and sharp density and dynamic pressure decrease (see under the lighter shading in Figure 10d) but no magnetic field signature; therefore it is unclear whether this variation is correlated with the passage of the same discontinuity. Figure 13b shows the orientation of the discontinuity front. We believe that the plotted fronts accurately describe this discontinuity because the predicted delays between spacecraft using equation (1) were very accurate when compared with the measured delays. The cone angle of the normal vector at Geotail is 48° and at IMP 8 and Interball ~15°; therefore this discontinuity fails the large cone angle condition. It also fails the converging convection electric field condition, since the convection electric field is in the same direction both sides of the discontinuity and is mostly parallel to it (similar to the cartoon of Figure 13a). This discontinuity therefore will not create a HFA or a foreshock cavity, and we predict that it will not create a ground transient either. Looking at the ground magnetometer data in Figure 8 we see a small transient perturbation at ~1915 UT and an even smaller one at ~1920 UT. It is unclear if either of these transients is triggered by the discontinuity. They are certainly not coherent between stations and there is no propagation pattern. It is possible that the short density and flux pulse registered at Geotail and Interball, respectively, do trigger the small transient, but since the right conditions are not satisfied for the discontinuity to interact with the bow shock creating a HFA or foreshock cavity there is no coherent and propagating, TCV-like transient on the ground.

4.3. Discontinuity 3 at 1925 UT

[47] This discontinuity has no |B| variation, only a rotation of the magnetic field in the XZ plane. There is no clear plasma signature in the three solar wind spacecraft. The discontinuity propagates from IMP 8 to Interball and then to Geotail and we estimate the time delays between spacecraft accurately with the use of equation (1) and the boundary orientations shown in Figure 13c. This looks like a well-behaved and predicted rotational discontinuity.

[48] The discontinuity fails both the condition of a large cone angle (cone angle of the normal vector at Geotail is 32°) and the condition of converging and perpendicular convection electric field on the two sides of the discontinuity. It will therefore not interact with the bow shock to create a HFA or a foreshock cavity and we therefore predict that there will be no significant ground transient triggered by this discontinuity. Indeed, in Figure 8 there is no transient after 1925 UT and only a small, noncoherent one just before 1925 UT.

4.4. Discontinuity 4 at 1950 UT

[49] This discontinuity exhibits a decrease in |B| and B_z, a small increase in density, and variations in all velocity components. It propagates from IMP 8 to Geotail and then to Interball. Figure 13d shows the orientation of the determined boundaries and their normal vectors, and it well explains the observed propagation pattern. The predicted time delays between spacecraft are also very accurate. This is again a well-defined and predicted discontinuity.

[50] This discontinuity also fails both the large cone angle conditions (cone angle of the normal vector at Geotail is 22°) and the convection electric field conditions that would enable it to create a HFA or a foreshock cavity at the bow shock. There is a small dynamic pressure enhancement associated, but it is only a 25% increase so we do not think that by itself it can trigger a transient (the dynamic pressure enhancement associated with the 1500 UT transient was a ~100%–200% enhancement). We therefore predict that there will be no significant ground transient triggered by this discontinuity. And indeed when we look at Figure 8 there is no perturbation after 1945 UT.

[51] In all four discontinuities described above, we were able to accurately predict if a ground transient would be triggered or not. On the basis of our results we suggest that only discontinuities that carry significant dynamic pressure enhancements or satisfy the conditions for creating a HFA or a foreshock cavity at the bow shock eventually trigger a ground transient with the TCV properties. Further studies are necessary to determine how general our results are.

5. Discussion and Conclusions

[52] It has not been possible, up to now, to establish a clear correlation between a particular solar wind and IMF feature and the occurrence of traveling convection vortices. The fact that solar wind data have been sparse, typically from only one spacecraft, and sometimes from less than ideal locations has significantly contributed to the lack of a successful and consistent correlation. Nevertheless, it is generally accepted that the trigger source of TCVs is in the solar wind, implying that the correct feature has not been found yet. To complicate matters more, the solar wind and IMF are largely disorganized with continuous random variations and in the rare occasions that a prior study had successfully identified a single solar wind trigger [e.g., *Friis-Christensen et al.*, 1988; *Zesta et al.*, 1999] a question remained as to why some solar wind perturbations cause TCVs and others not. So if the correct source of TCVs is understood, one should be able to also predict which solar wind disturbances would trigger a TCV and which ones would not.

[53] Recent work [*Sibeck et al.*, 1999; *Sitar et al.*, 1998; *Sibeck et al.*, 2002; *Lin*, 1997] has shed some light on the problem by identifying the bow shock as a key component. Specifically, it was found that the interaction of some types of discontinuities with the bow shock under the right conditions leads to the creation of HFAs or foreshock cavities [*Thomas et al.*, 1991; *Thomsen et al.*, 1988; *Schwartz et al.*, 2000; *Sibeck et al.*, 2002] which then launch dynamic pressure disturbances that propagate through the magnetosheath to subsequently trigger TCVs. It is unclear what percentage of TCVs are created by bow shock events and what percentage by pristine solar wind disturbances (or for that matter if the trigger source is in the solar wind at all), but it has become clear that one can not understand the sources of TCVs without considering bow shock properties.

[54] In the present paper we looked in detail at the solar wind data for two TCV events that occurred on 25 July 1997 at ~1500 UT and ~1835 UT. We had the fortuitous conjunction of four spacecraft, WIND, Geotail, Interball, and IMP 8, near the magnetosphere, so we were able not only to identify the discontinuity that triggered the TCV but also able to track the exact propagation of the discontinuity

in the solar wind and thus explain the creation and propagation of the transient in the magnetosphere and on the ground.

[55] We found that the 1500 UT TCV was triggered by the dynamic pressure enhancement carried by a tangential discontinuity that locally compressed the magnetopause generating the field-aligned currents that gave rise to the TCV in the ionosphere. Because the TD front had a spiral orientation, it hit the magnetosphere first in the afternoon region and then propagated toward the morning hours as it advected antisunward with the solar wind. We were able to accurately and quantitatively predict the propagation of the discontinuity between the four spacecraft. This explained the fact that the TCV was created in the early afternoon region and it then propagated westward, first toward local noon and then away from local noon. It also explained the westward propagation of the compression in the magnetosphere as observed by the GOES 8 and 9 spacecraft. We concluded that this TCV was the result of a pristine solar wind disturbance that carried its own dynamic pressure enhancement.

[56] The study of the trigger of the 1835 UT TCV turned out to be more complicated, and our results here are more suggestive rather than conclusive. During this TCV, WIND was inside the magnetosheath. We identified a discontinuity at all four spacecraft that we believe was responsible for the TCV. This was not a standard MHD discontinuity but rather a more complicated discontinuity with significant small-scale spatial structure and with leading and trailing edges whose separation diminished as the discontinuity propagated. The propagation pattern of this discontinuity was also unexpected but we were able to explain it, albeit only qualitatively. Our quantitative prediction of time delays between spacecraft was unsuccessful due to the less accurate definition of the discontinuity orientation. Our analysis suggests that this discontinuity interacted with the bow shock to create either an HFA or a foreshock cavity that then triggered the ground TCV, although we were unable to prove such an interaction due to the limitations of our data. We were thus able to suggest a solution that explains the apparent discrepancy in the observations between the three solar wind monitors (Geotail, Interball, and IMP 9), the magnetosheath monitor (WIND), and the magnetospheric spacecraft (GOES 8 and 9). Specifically, the three solar wind monitors indicated that there was a small dynamic pressure enhancement (only a $\sim$25% increase) associated with the discontinuity, so one might assume that it was the TCV trigger. However, WIND and the GOES spacecraft clearly showed that a dynamic pressure depression was responsible for the TCV. That led us to believe that a cavity created at the bow shock was likely responsible for that dynamic pressure depression and it was thus the actual trigger of the TCV. We were able to show that this discontinuity satisfied the conditions for the creation of a HFA from its interaction with the bow shock, namely the unit vector normal to the front had large cone angle and the convection electric field pointed toward the discontinuity front from both sides.

[57] The limitation of our interpretation comes from the fact that none of the three solar wind monitors detected all the typical HFA characteristics (there was no reduction in the magnetic field and density and no deflected flows). Our observations are thus not conclusive. It is possible that an HFA or cavity never formed or that if it did our spacecraft were not at the right time and right place to observe the right features. Of these two options we chose to consider the latter, mainly because of the geosynchronous and ground observations, which would be consistent with the creation of a foreshock cavity and inconsistent with the solar wind properties of the discontinuity (had an interaction with the BS not taken place). Then the 1835 UT discontinuity could be a nondeveloped HFA. Low densities and depressed magnetic fields are created by the expansion of the hot backstreaming reflected (at the bow shock) ion flows that excavate the cavity. This process needs time [*Thomas et al.*, 1991] and maybe there was not enough time in this case. An indication that that might be the case is the fact that temperatures (not shown) are indeed higher inside the discontinuity. Another explanation could be that the spacecraft are not close enough to the bow shock to be in the region of the excavated cavity, so they simply observe the hot reflected population. Since we have established that the bow shock was clearly involved in the generation of the TCV trigger, the only other explanation would be that there are other bow shock processes (other than HFA or foreshock cavities) that would launch dynamic pressure depressions in the magnetosheath and thus trigger TCVs [e.g., *Lin*, 1997].

[58] In summary, we concluded that in the first case it was the dynamic pressure enhancement (an increase of $\sim$100%–200%), a pristine solar wind feature, carried by a tangential discontinuity that triggered the ground TCV, while in the second case (a less clear event), the likely trigger was the interaction of a more complicated, non-MHD discontinuity with the bow shock that created a HFA or foreshock cavity that launched a dynamic pressure depression that subsequently triggered the ground TCV.

[59] Finally, we considered all the discontinuities (a total of four) in the 2-hour period surrounding the second TCV and were able to understand why none of these four discontinuities were able to trigger a ground TCV. We found that none of the discontinuities carried with it a sufficient dynamic pressure enhancement (no more than a 25% increase), and additionally none of them satisfied the conditions for creating a HFA or a foreshock cavity at the bow shock that could by itself trigger a TCV.

[60] It appears from our present study that a solar wind discontinuity needs to carry a dynamic pressure enhancement of at least 100% increase, or alternatively it needs to satisfy the conditions for creating a HFA or a foreshock cavity at the bow shock in order to be able to successfully trigger a TCV.

[61] Further work is necessary for a larger number of events for which a clear TCV is observed on the ground and solar wind and IMF data are available by more than three spacecraft well placed near the magnetosphere and the bow shock, in order to determine how general the results of the present work are and whether all TCVs have an easily identified trigger in the solar wind. Then the percentages of TCVs triggered by pristine solar wind disturbances and those triggered by bow shock processes can be quantified. It is important to understand how important the bow shock is in such processes. The percentages of HFA or foreshock cavities that trigger TCVs also need to be quantified.

Finally, it is necessary to understand whether the ground transients triggered by foreshock cavities or HFAs are fundamentally different from the ones triggered by disturbances that are advected in the solar wind.

[62] **Acknowledgments.** This work was supported by NSF grants ATM-9803800 and 0100902 at UCLA and by NSF grants ATM-0096534 and 9803800 at the Applied Physics Laboratory. GEOTAIL magnetic field data were provided by S. Kokubun through DARTS at the Institute of Space and Astronautical Science (ISAS) in Japan. GEOTAIL plasma data were provided by L. Frank through the University of Iowa GEOTAIL CPI instrument database. IMP 8 plasma data were taken by the CDAWEB database. The authors thank A. Szabo from NASA-GSFC for providing the high time resolution magnetic field data for IMP 8 and WIND, T. Phan from University of California, Berkeley for providing the WIND 3dp plasma data, J. Safrankova for the Interball VDP data, S. Romanov for the Interball magnetic field data, H. Singer from NOAA-SEC for the GOES data, J. Hughes for the MACCS data, J. Samson for the CANOPUS data, and J. Waterman for the Greenland magnetometer data.

[63] Arthur Richmond thanks Eigil Friis-Christensen and Steven J. Schwartz for their assistance in evaluating this paper.

References

Fairfield, D. H. (1971), Average and unusual locations of the Earth's magnetopause and bow shock, *J. Geophys. Res.*, *76*, 6700.

Frank, L. A., K. L. Ackerson, W. R. Paterson, R. L. Dyson, G. T. Parmentier, and G. L. Pickett (1994), The Comprehensive Plasma Instrument (CPI) for the Geotail spacecraft, *J. Geomagn. Geoelectr.*, *46*, 23–37.

Friis-Christensen, E., M. A. McHenry, C. R. Clauer, and S. Vennerstrom (1988), Ionospheric traveling convection vortices observed near the polar cleft: A triggered response to sudden changes in the solar wind, *Geophys. Res. Lett.*, *15*, 253–256.

Glassmeier, K. H., M. Hönisch, and J. Untiedt (1989), Ground-based and satellite observations of traveling magnetospheric convection twin-vortices, *J. Geophys. Res.*, *94*, 2520–2528.

King, J. H. (1982), Availability of IMP-7 and IMP-8 data for the IMS period, in *The IMS Source Book: Guide to the International Magnetospheric Study Data Analysis*, edited by C. T. Russell and D. J. Southwood, pp. 10–20, AGU, Washington, D. C.

Kivelson, M. G., and D. J. Southwood (1991), Ionospheric traveling vortex generation by solar wind buffeting of the magnetopause, *J. Geophys. Res.*, *96*, 1661–1667.

Klimov, S., et al. (1997), ASPI-experiment: Measurements of fields and waves onboard the Interball-1 spacecraft, *Ann. Geophys.*, *15*, 514–527.

Kokubun, S., T. Yamamoto, M. H. Acuna, K. Hayashi, K. Shiokawa, and H. Kawano (1994), The Geotail Magnetic Field Experiment, *J. Geomagn. Geoelectr.*, *46*, 7–21.

Konik, R. M., L. J. Lanzerotti, A. Wolfe, and C. G. Maclennan (1994), Cusp latitude magnetic impulsive events: 2. Interplanetary magnetic field and solar wind conditions, *J. Geophys. Res.*, *99*, 14,831.

Lazarus, A. J., and K. I. Paularena (1997), A comparison of solar wind parameters from experiments on the IMP 8 and Wind spacecraft, in *Measurement Techniques in Space Plasmas: Particles*, *Geophys. Monogr. Ser.*, vol. 102, edited by R. F. Pfaff, J. E. Borovsky, and D. T. Young, pp. 85–90, AGU, Washington, D. C.

Lepping, R. P., et al. (1995), The Wind magnetic field investigation, *Space Sci. Rev.*, *71*, 207–229.

Lin, R. P., et al. (1995), A three-dimensional plasma and energetic particle investigation for the Wind spacecraft, *Space Sci. Rev.*, *71*, 125–153.

Lin, Y. (1997), Generation of anomalous flows near the bow shock by its interaction with interplanetary discontinuities, *J. Geophys. Res.*, *102*, 24,265–24,282.

Lin, Z.-M., E. A. Bering, J. R. Benbrook, B. Liao, L. J. Lanzerotti, C. G. Maclennan, A. N. Wolfe, and E. Friis-Christensen (1995), Statistical studies of impulsive events at high latitudes, *J. Geophys. Res.*, *100*, 7553–7566.

Lysak, R. L., Y. Song, and D. H. Lee (1994), Generation of ULF waves by fluctuations in the magnetopause position, in *Solar Wind Sources of Magnetospheric ULF Waves*, *Geophys. Monogr. Ser.*, vol. 81, edited by M. J. Engebretson, K. Takahashi, and M. Scholer, pp. 273–281, AGU, Washington, D. C.

Murr, D. L., W. J. Hughes, A. S. Rodger, E. Zesta, H. U. Frey, and A. T. Weatherwax (2002), Conjugate observations of traveling convective vortices: The field-aligned current system, *J. Geophys. Res.*, *107*(A10), 1306, doi:10.1029/2002JA009456.

Roelof, E. C., and D. G. Sibeck (1993), Magnetopause shape as a bivariate function of interplanetary magnetic field Bz and solar wind dynamic pressure, *J. Geophys. Res.*, *98*, 21,421.

Šafránková, J., G. Zastenker, Z. Nemecek, A. Fedorov, M. Simersky, and L. Prech (1997), Small scale observations of magnetopause motion: Preliminary results of the INTERBALL project, *Ann. Geophys.*, *15*, 562–569.

Schwartz, S. J., G. Paschmann, N. Sckopke, T. M. Bauer, M. Dunlop, A. N. Fazarkerley, and M. F. Thomsen (2000), Conditions for the formation of hot flow anomalies at Earth's bow shock, *J. Geophys. Res.*, *105*, 12,639–12,650.

Sibeck, D. G., and G. I. Korotova (1996), Occurrence patterns for transient magnetic field signatures at high latitudes, *J. Geophys. Res.*, *101*, 13,414–13,428.

Sibeck, D. G., et al. (1999), Comprehensive study of the magnetospheric response to a hot flow anomaly, *J. Geophys. Res.*, *104*, 4577–4593.

Sibeck, D. G., T.-D. Phan, R. Lin, R. P. Lepping, and A. Szabo (2002), Wind observations of foreshock cavities: A case study, *J. Geophys. Res.*, *107*(A10), 1271, doi:10.1029/2001JA007539.

Siscoe, G. L., L. Davis Jr., P. J. Coleman Jr., E. J. Smith, and D. E. Jones (1968), Power spectra and discontinuities of the interplanetary magnetic field: Mariner 4, *J. Geophys. Res.*, *73*, 61–82.

Sitar, R. J., C. R. Clauer, and E. Friis-Christensen (1996), High-latitude ground-based response to sudden changes in solar wind dynamic pressure, *J. Geophys. Res.*, *101*, 27,001–27,013.

Sitar, R. J., et al. (1998), Multi-instrument analysis of the ionospheric signatures of a hot flow anomaly occurring on July 24, 1996, *J. Geophys. Res.*, *103*, 23,357–23,372.

Sonnerup, B. U. Ö., and L. J. Cahill Jr. (1967), Magnetopause structure and attitude from Explorer 12 observations, *J. Geophys. Res.*, *72*, 171.

Thomas, V. A., D. Winske, M. F. Thomsen, and T. G. Onsager (1991), Hybrid simulation of the formation of a hot flow anomaly, *J. Geophys. Res.*, *96*, 11,625–11,632.

Thomsen, M. F., J. T. Gosling, S. J. Bame, K. B. Quest, C. T. Russell, and S. A. Fuselier (1988), On the origin of hot diamagnetic cavities near the Earth's bow shock, *J. Geophys. Res.*, *93*, 11,311–11,325.

Zesta, E., W. J. Hughes, M. J. Engebretson, T. J. Hughes, A. J. Lazarus, and K. I. Paularena (1999), The November 9, 1993 traveling convection vortex event: A case study, *J. Geophys. Res.*, *104*, 28,041.

D. G. Sibeck, NASA Goddard Space Flight Center, Code 696, Greenbelt, MD 20771, USA. (dsibeck@lepvax.gsfc.nasa.gov)

E. Zesta, Department of Atmospheric Sciences, University of California, Los Angeles, 7127 Math Sciences, Box 951565, Los Angeles, CA 90095-1565, USA. (ezesta@atmos.ucla.edu)